X-ray Variability of the Magnetic Cataclysmic Variable V1432 Aql and the Seyfert Galaxy NGC 6814

K. Mukai[1,2]

Code 662, NASA/Goddard Space Flight Center, Greenbelt, MD 20771, USA

mukai@milkyway.gsfc.nasa.gov

C. Hellier

Department of Physics, Keele University, Keele, Staffordshire ST5 5BG, United Kingdom

G. Madejski

Stanford Linear Accelerator Center, Glast Group, 2575 Sand Hill Road, MS 43A, Menlo Park, CA 94025, USA

J. Patterson

Department of Astronomy, Columbia University, 538 W. 120th Street, New York, NY 10027, USA

and

D.R. Skillman

Center for Backyard Astrophysics (East), 9517 Washington Avenue, Laurel, MD 20723, USA

ABSTRACT

V1432 Aquilae (=RX J1940.2−1025) is the X-ray bright, eclipsing magnetic cataclysmic variable $\sim 37'$ away from the Seyfert galaxy, NGC 6814. Due to a 0.3% difference between the orbital (12116.3 s) and the spin (12150 s) periods, the accretion geometry changes over the ∼50 day beat period. Here we report the results of an *RXTE* campaign to observe the eclipse 25 times, as well as

[1]Also Universities Space Research Association

[2]Also Columbia Astrophysics Laboratory, Columbia University, 550 West 120th Street, New York, New York 10027, USA

of archival observations with *ASCA* and *BeppoSAX*. Having confirmed that the eclipse is indeed caused by the secondary, we use the eclipse timings and profiles to map the accretion geometry as a function of the beat phase. We find that the accretion region is compact, and that it moves relative to the center of white dwarf on the beat period. The amplitude of this movement suggest a low-mass white dwarf, in contrast to the high mass previously estimated from its X-ray spectrum. The size of the X-ray emission region appears to be larger than in other eclipsing magnetic CVs. We also report on the *RXTE* data as well as the long-term behavior of NGC 6814, indicating flux variability by a factor of at least 10 on time scales of years.

Subject headings: Stars: binaries: eclipsing — stars: novae, cataclysmic variables — stars: individual (V1432 Aql) — galaxies: Seyfert — galaxies: individual (NGC 6814) — X-rays: binaries — X-rays: galaxies

1. Introduction

The Seyfert galaxy NGC 6814 became famous with the apparent discovery, made with the non-imaging *EXOSAT* Medium-energy Experiment (ME), that its X-ray flux was modulated with a strict ∼12,150 s period (Mittaz & Branduardi-Raymont 1989). However, this fame turned into notoriety when it was discovered, through imaging X-ray observations with *ROSAT* Position Sensitive Proportional Counter (PSPC), that this periodicity actually belonged to another X-ray source in the field of view, RX J1940.1−1025, about 37′ away from NGC 6814 (Madejski et al. 1993; Staubert et al. 1994). The latter authors identified this new X-ray source with a V∼16 mag object, subsequently designated V1432 Aquilae, and proposed that it was a cataclysmic variable (CV) system belonging to the polar sub-class (also known as AM Her-type systems).

A CV is a semi-detached binary in which the white dwarf primary accretes mass from a late-type (usually an M dwarf) secondary. In a polar (see Cropper 1990 for a review), the primary is strongly (≥10 MGauss) magnetic, which prevents the formation of an accretion disk. The accretion flow is channeled by the magnetic field towards the magnetic pole region(s), where a strong standing shock forms. The post-shock plasma cools by emitting optical/infrared cyclotron emission and optically thin thermal X-ray emission with a typical temperature of kT∼10 keV ("the hard component"). The white dwarf surface is heated from above by these radiation, and probably directly by dense blobs whose shocks are buried within the white dwarf atmosphere, and emit optically thick, blackbody-like emission with a typical temperature of kT∼30 eV ("the soft component"). In most polars, the soft X-ray

component dominates over the hard, although in some the two are roughly comparable.

In polars, the strong magnetic field of the primary usually synchronizes the white dwarf spin to the orbital period. In the other subclass of magnetic CVs, intermediate polars (IPs) or DQ Her-type systems (see Patterson 1994 for a review), the spin period of the white dwarf (P_{spin}) is significantly shorter than the orbital period (P_{orb}), many of them with $P_{spin} \sim 0.1$ P_{orb}. In IPs, a weaker magnetic field or a greater orbital orbital separation is thought to prevent synchronism, and that their current P_{spin} is close to their evolutionary equilibrium.

V1432 Aql is among the minority of polars with a strong hard X-ray component. Moreover, two almost identical periods have been found in this system (Patterson et al. 1995; Friedrich et al. 1996). The orbital period is 12116.3 s, while the second period is ∼0.3% longer at 12150 s, with a resulting beat period ($P_{beat}^{-1} = P_{orb}^{-1} - P_{spin}^{-1}$) of ∼50 days. This makes V1432 Aql an asynchronous polar, in which P_{spin} and P_{orb} differ by ∼1%, probably in a temporary departure from synchronism. In the first known example, V1500 Cyg (=Nova Cygni 1975), the nova explosion is the almost certain cause of the asychronism. In an asynchronous polar, a strong (≫accretion torque) MHD torque should operate to synchronize the white dwarf spin on a short (≪evolutionary) time scale, and indeed this is observed in V1500 Cyg (synchronization timescale ∼150 years; Schmidt et al. 1995). In addition to V1500 Cyg, BY Cam and CD Ind are also asynchronous with P_{spin} being $\sim 1\%$ shorter than P_{orb}. On the other hand, V1432 Aql appears to be asynchronous in the other direction. Mukai (1998) questioned if this was possible, and also pointed out that such a system might be expected to synchronise much more quickly than V1500 Cyg like systems: When $P_{orb} > P_{spin}$, the synchronization must compete and overcome the accretion torque, whereas when $P_{orb} < P_{spin}$, they cooperate. Although Schmidt & Stockman (2001) showed that it was possible for a nova explosion to slow down the white dwarf spin, thus producing a V1432 Aql-like system, the synchronization timescale of V1432 Aql that Geckeler & Staubert (1997) inferred is 100 yrs, comparable to that of V1500 Cyg.

Mukai (1998) proposed an alternative model in which P_{spin} is about 4040 s. A complex interaction of spin and orbital periodicity, and less than perfect observational sampling could explain the apparent presence of a 12150 s period. However, we now consider this model unlikely, given the confirmation of rapid timescale for synchronization (§4.1). We will therefore refer to the 12150 s period as the spin period in the rest of this paper.

There is a second controversy surrounding V1432 Aql. The fiducial marker that defines the 12116.3 s orbital period is an eclipse-like event seen both in the optical and X-ray light curves. However, Watson et al. (1995) argued this to be a dip caused by the accretion stream, as seen in several well-observed polars (King & Williams 1985). They based this conclusion partly on the light curve which is unusual for an eclipsing polar, but mainly on the

residual X-ray flux observed with non-imaging *Ginga* Large Area Counter (LAC) detector. The observed spectrum became harder during the eclipse, which suggested a photoelectric absorption event by the accretion stream. However, the presence and the regularity of the same feature at all energies strongly argues that this is a true eclipse by the secondary star (Patterson et al. 1995). In this paper, we show that later X-ray observations are consistent with zero residual flux, thus strongly favoring the eclipse interpretation. We then go on to use the eclipse as a tool to explore the accretion geometry as a function of the beat phase.

Although not the origin of the ~ 12000 s period, the Seyfert galaxy NGC 6814 is by no means an uninteresting object. In the optical, it shows broad emission lines of only modest width ($\sigma \sim 3000$ km s^{-1}); both the continuum (Doroshenko 1988) and the emission lines (Sekiguchi & Menzies 1990) are highly variable, varying between Seyfert 1 or Seyfert 1.8 classifications. The *ROSAT* observations show that the X-ray flux of NGC 6814 is also variable, decreasing by a factor of at least 5 between October 1992 and October 1993, and by a factor of 2 in ~ 6 hours (König et al. 1997). Given the angular separation of $\sim 37'$ between V1432 Aql and NGC 6814, X-ray data with non-imaging, collimated instruments are often entangled; the strong variability of NGC 6814 then leads to require particular care to be taken when observing V1432 Aql with such an instrument. Therefore, although V1432 Aql is the primary focus of this work, we also present results on the X-ray behaviors of NGC 6814, both as a necessary precondition for the study of the CV and as a worthy goal in itself.

We describe the X-ray observations in §2. We present the results and implication on NGC 6814 in §3. The results on V1432 Aql (including a short summary of continued optical photometry) are presented in §4, and discussed in §5. A summary of conclusions is given in §6.

2. X-ray Observations

In addition to our own *RXTE* campaign, we have analyzed archival observations with two X-ray observatories with imaging telescopes. All X-ray observations analyzed here were obtained during 1997 and 1998.

2.1. *BeppoSAX* Observations

V1432 Aql was observed on 8 occasions between 1997 April 2 and May 13 with *BeppoSAX* (Boella et al. 1997a). Here we will focus on the data from Medium Energy Con-

centrator Spectrometer (MECS) instruments (Boella et al. 1997b). *BeppoSAX* carried 3 identical units of MECS, but one had malfunctioned between the 7th and 8th observations of V1432 Aql, so the last observation was made with only two operational MECS. Each visit resulted in between 8 and 13 ksec of effective exposure with the MECS. Details of the 8 observations are listed in Table 1.

Although the Low Energy Concentrator Spectrometer (LECS) can in principle provide information regarding the behavior of the source below 2 keV, the data quality is lower than the MECS because there is only one unit of LECS and it is operated only during orbital night. Moreover, the latter means that LECS data sample a subset of the phase covered by MECS data. Given the potential complications from cycle-to-cycle variability, we have opted not to include LECS data in our analysis. Similarly, we have not included data from the two non-imaging narrow-field instruments on-board *BeppoSAX*, the High Pressure Gas Scintillation Proportional Counter and the Phoswich Detection System.

We have extracted source counts from the MECS data using a circular extraction region with a radius of 3.6 arcmin, and background counts from an annular extraction region with outer and inner radii of 16.9 and 7.2 arcmin, respectively, assumed that the background was flat, and therefore scaled the latter by the ratio of areas of the extraction regions to derive the net source count rates. We have extracted light curves from PI channels 31–100 ($\sim$1.5–4.5 keV) and channels 101–170 ($\sim$4.5–8.0 keV) with a bin size of 16 s. Roughly speaking, these two bands contain equal counts from V1432 Aql, and when combined, result in the highest signal-to-noise.

2.2. A Serendipitous *ASCA* Observation

V1432 Aql was observed serendipitously with *ASCA* in 1997 October during the observation of a high redshift quasar, PKS 1937−101 (see Table 1 for further details). Although *ASCA* has 4 co-aligned telescopes (Tanaka et al. 1994), V1432 Aql was about 20 arcmin off-axis and was not in the field of view of the two Solid-state Imaging Spectrometers. As for the two Gas Imaging Spectrometers (GIS), the source was too close to the on-board radioactive calibration source in GIS-3 for a useful analysis. We therefore restrict ourselves to the GIS-2 data.

We have extracted the source counts from an elliptical extraction region (to match the overall shape of the off-axis point spread function) with semi-major and semi-minor axes of 7.5 and 2.9 arcmin, respectively. Background was taken from a large area of the detector with a similar off-axis angle as the source, which was then subtracted from the source data after

scaling with the ratio of the detector areas. We have used two energy bands, PI channels 60–169 (0.7–2 keV) and 170–847 (2–10 keV) for the *ASCA* data.

2.3. The *RXTE* Campaign

We have performed a series of 25 observations between 1998 May 18 and 1998 Aug 21, covering approximately two beat cycles of V1432 Aql with *RXTE* (Bradt et al. 1993). Each observation covers a small range of orbital phase of V1432 Aql, centered on the eclipse. Here we concentrate on the data obtained with the Proportional Counter Array (PCA) (Jahoda et al. 1996).

The angular separation of V1432 Aql and NGC 6814 of ∼37 arcmin means that PCA observations pointed at V1432 Aql have some sensitivity to the X-ray photons from NGC 6814. We have therefore chosen to offset our pointing by ∼15′ (position "C" in Table 2 and in Figure 1). We estimate that the PCA collimater response is about 80% for V1432 Aql and about 10% for NGC 6814 at position C. Furthermore, we wished to monitor the X-ray flux level of NGC 6814 to assess the residual contamination, and for its own scientific merits. Our intention was to similarly offset the pointing. However, due to a typographical error on our part, the actual pointings were performed at position A in Table 2 and in Figure 1 (change the minute figures of RA to 43 and we would have achieved our original aim; position A' in Figure 1). This greatly reduced the effectiveness of our campaign for NGC 6814 (see, however, §3).

Each of the 25 observations was composed of a pointing at position C preceded by, followed by, or in two cases sandwiched between, a pointing at position A (see Figure 2 for a couple of examples). Typically 2 ksec of good data were obtained at position C. The details of the *RXTE* observations are given in Table 3. As is often the case, not all of the five Proportional Counter Units (PCUs) were active in all observations: the active PCUs are also indicated in the table. The collimator response at off-axis positions are a function of the roll angle, since the collimator geometry is hexagonal. We have estimated the actual efficiency achieved in each C pointing for V1432 Aql and for NGC 6814, so that we can infer the on-axis count rates (per second per PCU) from the observed rates. We have estimated the background using faint source background model, using files pca_bkgd_faint240_e03v03.mdl and pca_bkgd_faintl7_e03v03.mdl as well as the South Atlantic Anomaly history file. This model is highly successful in reproducing the non-X-ray background experienced by the PCA. However, it only models the average, high-latitude, cosmic X-ray background, which is not appropriate for this part of the sky. Moreover, the model does not include the contamination by NGC 6814.

We have extracted data from the top layer of the PCA, which gives the best signal-to-noise ratio. For the study of NGC 6814, we use the entire energy band of the PCA (effectively 3–15 keV), while for the detailed study of the eclipses in V1432 Aql, we restrict ourselves to channels 8–27, or roughly 3–10 keV, which on average improves the signal-to-noise ratio. In both cases, we use count rate per PCU in our plots to account for the variable number of active PCUs, and moreover convert this to the estimated on-axis rate for the appropriate target.

3. X-ray Variability of NGC 6814

3.1. The Medium Energy X-ray Light Curves of NGC 6814

We now use our *RXTE* campaign as well as archival data to evaluate the X-ray fluxes of NGC 6814 in the 2–10 keV band. Lower energy X-rays from NGC 6814 have been securely detected using imaging instruments and are known to be variable, starting with the *Einstein* Imaging Proportional Counter (IPC) observation spanning two days, which showed this source to be variable on a timescale of 20,000 s (Tananbaum 1980). A long-term light curve obtained with *EXOSAT* Low-energy Experiment (LE) is presented in Figure 1 of Mittaz & Branduardi-Raymont (1989); and for *ROSAT* results, see König et al. (1997). As Mittaz & Branduardi-Raymont (1989) noted, the *EXOSAT* Medium-energy Experiment (ME) data of "NGC 6814" varied in a manner similar to that of the LE data over the timescale of months (their Figure 1). Although we now know that the (non-imaging) ME data were contaminated with X-rays from V1432 Aql, as evidenced by the detection of the 12,000 s signal, the LE–ME correlation is a strong evidence that a significant fraction of the observed ME counts did originate from NGC 6814.

In our *RXTE* campaign, we attempted to monitor the X-ray variability of NGC 6814 by obtaining data at position "A" as well as at position "C." Although our typographical error made it less effective than we had hoped for, we believe we have securely detected NGC 6814 during two pointings, on 1998 May 18 and on 1998 June 16. The light curves on these two dates at both pointing positions are plotted in Figure 2. In both cases, the curve is flat at position "A" at a level higher than the adjacent section of light curve taken at "C." We also show, in Figure 3, the spectra on 1998 May 18 taken at these two pointing positions. The "A" spectra on May 18 and June 16 can both be fit with a single power law without an obvious Fe Kα line, with a photon index of $\sim$1.9. The inferred 2–10 keV fluxes were 3.4 and 4.9 $\times 10^{-11}$ ergs cm^{-2}s^{-1}, respectively, although this assumes all the photons were from the NGC 6814 (the actual fluxes were probably somewhat lower, since some contamination by V1432 Aql is likely).

We have another method to estimate the X-ray flux from NGC 6814. By interpreting the mid-eclipse residual count rates from "C" observations (see §4.3 for details) as off-axis contribution from NGC 6814, we have constructed its light curve during our *RXTE* campaign (Figure 4), although we cannot rule out other contributors to the mid-eclipse counts (including residual flux in V1432 Aql itself). On the two dates where the "A" pointing securely detected NGC 6814, the count rates measured by this method are somewhat lower, and in fact may be more realistic. Other points on this curve lack independent confirmations, but nevertheless may be considered an estimate of the level of the 2–10 keV flux variability of NGC 6814 during the *RXTE* campaign.

Since the 2–10 keV flux indicated for NGC 6814 in 1998 appeared much higher than expected, given the *ROSAT* results (König et al. 1997), we have investigated the long-term flux history of this object further. The most reliable determination of its 2–10 keV flux can be obtained from the 1993 May *ASCA* observation: the source was detected at 0.044 cts s^{-1} in the GIS, had a power law spectrum with a photon index of 1.7 and Galactic absorption (9.8×10^{20} cm^{-2}; Elvis et al. 1989) and a 2–10 keV flux of 1.7×10^{-12} ergs cm^{-2}s^{-1}. We use this spectral shape to infer 2–10 keV flux from lower-energy imaging observations (*Einstein* IPC and High Resolution Imager observations in 1979 April, *EXOSAT* LE observations in 1983–1985, the *ROSAT* all-sky survey data in 1990, and pointed *ROSAT* PSPC observations in 1992 and 1993). Although extrapolation can lead to inaccuracies, if the spectral shape was different (e.g., with a soft excess) during any of these observations, our estimates are probably accurate to within a factor of 2. We also note that NGC 6814 was detected at 0.36 cts s^{-1} in the *ROSAT* All-Sky Survey (http://www.rosat.mpe-garching.mpg.de/survey/rass-bsc/; the observation dates were estimated using the formula given in Verbunt et al. 1997). This extends the range of PSPC count rates of NGC 6814 to a full order of magnitude from a factor of 5 noted by König et al. (1997). In Figure 5, we plot the reconstructed flux history of NGC 6814, including, additionally, the two most reliable (but also among the brightest) values from our *RXTE* campaign, and two additional points based on mid-eclipse flux during the 1989 and 1990 *Ginga* observations. This shows a wide range in estimated flux, from $\sim 1.0\times10^{-12}$ to $> 1.0\times10^{-11}$ ergs cm^{-2}s^{-1}. The highest point is based on *EXOSAT* LE rate of 0.0225 cts s^{-1} on 1983 September 4, at an estimated 2–10 keV flux of 3.3×10^{-11} ergs cm^{-2}s^{-1}, which accounts for most of the ME count rates observed on that occasion. In the 1985 October 16 observation in which the 12,000 s period was discovered, we estimate that NGC 6814 at $\sim 1.0\times10^{-11}$ ergs cm^{-2}s^{-1} (2–10 keV), and infer that the observed ME counts were roughly half from the AGN and half from the CV. This is consistent with the fact that ME count rate never dropped below $\sim$0.8 cts s^{-1}, even during the eclipse of V1432 Aql.

Finally, we estimate that our *RXTE* observing strategy was successful in greatly reducing the NGC 6814 contributions to the count rates when our intended target is V1432 Aql.

Figure 4, multiplied by the collimator efficiency for NGC 6814 for each C poiting (∼0.1), can be interpreted as the upper limit to the contamination level due to NGC 6814. The AGN and the Galactic X-ray background prevent us from setting a strict upper limit to the flux at mid-eclipse to better than ∼0.15 cts s^{-1} per PCU.

3.2. Implications for the Nature of NGC 6814

NGC 6814 is a Seyfert galaxy that shows strong variability of optical continuum and lines over timescales of months and longer (see, e.g., Sekiguchi & Menzies 1990). Our work suggests that it also shows a strong variability in its X-ray flux over timescales of months and years. The variability level seen in Figure 5 is comparable to that seen in the well-studied Seyfert galaxies such as NGC 4051 (see, e.g., Peterson et al. 2000), IRAS 13224−3809 (Boller et al. 1997) or Akn 564 (Turner et al. 2001).

NGC 6814 also shows strong, shorter-term X-ray variability, by a factor of 3 in 8 hours (König et al. 1997; see also Tananbaum 1980). Our new *RXTE* data also show strong variability on time scales of days, indicating such a behavior is quite common. Given this rapid variability in the optical and X-ray bands, and the relatively modest width of the emission lines, we suggest that it probably belongs to the class of Narrow Line Seyfert 1 (NLS1) galaxies (for an overview of X-ray properties of these objects and correlations of X-ray and optical properties, see, e.g., Boller et al. 1996). Since the emission lines are strongly variable, this source could have escaped proper identification, depending on its state when the census was taken. NLS1s often have complex X-ray spectra, with a hard X-ray continuum above ∼1 keV and a strong soft excess below, so it would be interesting to study its spectrum with an X-ray spectrometer with high and low energy sensitivities, such as *XMM-Newton*.

4. Results on V1432 Aql

4.1. Optical Photometry

The main features of the optical light curve of V1432 Aql were described by Patterson et al. (1995), which contains details of the 1993 and 1994 photometry campaigns. We have continued this coverage steadily through 2002, including a 140 day campaign in 1998 to support the *RXTE* observations, using primarily the telescopes of the Center for Backyard Astrophysics (CBA; Skillman & Patterson 1993). Details of these follow-up campaigns will be reported elsewhere. We make use of two key findings from the optical campaigns in

interpreting the X-ray data:

(1) The timings of the optical eclipses can be described by the following linear ephemeris in Heliocentric Julian Date on the UTC system:

$$Mid - eclipse = HJD2449199.693 + 0.14023475(5)E \quad (1)$$

This ephemeris is used throughout this paper in studying the eclipse and other orbital modulations.

(2) The spin period has been steadily decreasing through 1993–2002. We have measured the times of primary spin minima from light curves averaged over the 50-day beat cycle (to avoid contamination from the orbital variability), and report the results in Table 4. We plot the observed minus that calculated (O−C) times using a test linear ephemeris, $2449197.741 + 0.140613E$ (Figure 6). The parabola represents our best-fit quadratic spin ephemeris:

$$Spin - minimum = HJD2449197.741 + 0.140630E - 6.5 \times 10^{-10}E^2 \quad (2)$$

This equates to a period decrease with $\dot{P} = -(9 \pm 1) \times 10^{-9}$, confirming and extending the result of Geckeler & Staubert (1997). Their recent update of this result (Staubert et al. 2003) is also compatible with this level of spin-up. Such a rapid spin up shows that V1432 Aql is currently well away from spin equilibrium, thus strongly favoring the asynchronous polar model of V1432 Aql. This implies a synchronization time of 120±15 years, similar to that seen in other asynchronous polars. The beat period between the eclipse and spin periods was 52 days during our 1998 *RXTE* campaign.

4.2. Hard X-ray Orbital Modulation

We present the average orbital modulations of V1432 Aql observed with *BeppoSAX* MECS (see Table 1) in the left panels of Figure 7. Note that the 8 *BeppoSAX* observations were spread over the beat cycle, and therefore we might expect features that are persistent through the beat cycle to be prominent in this representation. The X-ray eclipse, seen at the phase of the optical eclipse as predicted by ephemeris (1), is deep and shows sudden transitions, which we will analyze in detail in §4.3 using the *RXTE* data. In addition, two energy-dependent dips can be seen. These dips are deeper in the 1.5–4.5 keV band than in the 4.5–8 keV band, hence show up as periods of enhanced hardness ratio [(4.5–8 keV)/(1.5–4.5 keV)]. The hardness exceeds 1.0 between orbital phase 0.17 and 0.24, and between 0.25

and 0.27; and between 0.56 and 0.72. Given these ranges, we will refer to these dips as being at orbital phase 0.2 and 0.65. Although the average intensity is lower immediately after the eclipse, the hardness ratio is lower at this phase, if anything, than the rest of the orbital cycle.

The average *BeppoSAX* MECS spectrum of V1432 Aql is typical of magnetic CVs in showing a hard continuum and the Fe Kα emission feature. The hardness of the continuum is indicative of a complex partial covering absorber (Done & Magdziarz 1998). Given this, and the presence of orbital, spin, and beat periods in V1432 Aql, the existing data are not good enough to allow a quantitative description of spectral changes beyond what can be seen from hardness ratio variations. In particular, although we note that the Fe Kα feature appears to be variable and that this potentially provides a useful tool, it is not even clear what period the lines are modulated on.

We have also folded the same *BeppoSAX* MECS data, excluding those taken during orbital phase 0.95–1.10, on the spin ephemeris (2) above, which we present in the right panels of Figures 7. While these light curves show strong variability, a systematic pattern is not obvious; moreover, the the spin-folded hardness ratio curve is more stable than the orbit-folded hardness ratio curve. We interpret this as indicating that the orbital modulation is more important in hard (>1.5 keV) X-rays than the spin modulation. While the latter is expected to be present at some level, we cannot claim detection of one in the *BeppoSAX* data. This is in contrast to the previous claims (Geckeler & Staubert 1997; Staubert et al. 2003) of X-ray spin modulation; note, however, these are based on *ROSAT* PSPC data, and may apply only to soft X-rays. We also note that the *BeppoSAX* observations are particularly well suited to discriminate between the orbital and spin phenomena in V1432 Aql. With a lesser coverage (typically lasting 0.5–3 days, much less than the beat period), an object which is modulated purely on the orbital period would show an apparent modulation when folded on the spin period. It is the combination of the 8 *BeppoSAX* observations, spread through a beat cycle, that enables us to show the relative importance of the orbital modulation.

Are the dips at orbital phases 0.2 and 0.65 persistent? To answer this question, we plot in Figure 8 the folded hardness ratio curves, which appear to be less affected by random variations than intensity curves, for each of the 8 *BeppoSAX* observations. Since each of the 8 observations was taken in 5–7 hrs, much shorter than the 50-day beat period, the orbital and spin folds are indistinguishable, apart from a constant phase offset. This offset changes from observation to observation; to guide the eye, we have indicated the location of spin phase 0.0 in each panel of Figure 8. Any feature fixed in the spin period of V1432 Aql should move to keep its position fixed relative to these vertical marks; we find no such feature. The phase 0.65 feature seen in Figure 7 is clearly detected in observations 2, 3, and 4, each within

orbital phase range 0.6–0.7. It is not strongly detected in observations 1 or 6, while the remaining 3 observations did not cover the relevant phase. The coverage of orbital phase 0.2 was poorer, but this feature clearly varied in strength between observations 1, 2, and 3.

In Figure 9, we present the folded *ASCA* GIS light curves in two energy bands, and their softness ratio (we chose this representation as the 0.7–2 keV count rates are consistent with zero at many orbital phases). This observation had a total duration of about 28 hrs, and hence this orbital fold can also be considered a spin fold with an offset. Although at lower quality, we confirm the total eclipse in the 2–10 keV band coincident with the optical eclipse. The behavior of V1432 Aql during this observation was similar to that it displayed during the *Ginga* observation (see Figure 13 of Watson et al. 1995). While the *ASCA* data show a minimum at the calculated phase of the optical spin minimum (shown as vertical lines), it is also at orbital phase 0.63. From *ASCA* data alone, we cannot tell if this is an orbital or a spin feature; however, given the persistence of orbital phase 0.65 feature in the *BeppoSAX* data, an orbital interpretation seems likely; the other minimum at orbital phase 0.2 is also reminiscent of the feature in Figure 7.

4.3. The Eclipse

We plot in Figure 10 the average eclipse profiles of V1432 Aql as observed with *BeppoSAX* MECS and with *RXTE* PCA, folded on ephemeris (1). They both show that X-ray eclipse is coincident with the optical eclipse, and has a flat-bottomed profile typical of total eclipse by the secondary. MECS count rate drops to $(1.0 \pm 1.4) \times 10^{-3}$ cts s^{-1} (mean and standard deviation) during the flat bottom, compared to $(6.0 \pm 2.6) \times 10^{-2}$ cts s^{-1} out-of-eclipse: this is a total eclipse with no detectable residual flux in the MECS 1.5-8 keV band. Examination of the energy-resolved eclipse curve is consistent with this, in particular there is no detectable residual flux in the harder (4.5–8 keV) band. The *RXTE* PCA curve bottoms out at 0.12 ± 0.13 cts s^{-1}. Since any residual flux at this level can be interpreted as due to contamination by NGC 6814 (see §3.1), our *RXTE* result is also consistent with a total eclipse in V1432 Aql. Given this, we believe that the "absorption dip" interpretation of Watson et al. (1995) is no longer tenable. We therefore proceed further with the interpretation that V1432 Aql shows a true eclipse by the companion star.

Visual inspection of the individual eclipse light curves shows that the ingress and the egress are usually very sharp, and can be located accurate to ∼2 s by eye (cf. Figure 2). However, the out-of-eclipse flux is too low in some pointings to provide reliable estimates (that is, the limiting factor appears to be the out-of-eclipse flux level, not the reliability of the particular method used to measure the timings). We have therefore attempted to measure

the eclipse timings by eye, and report the result in Table 5, together with the inferred eclipse widths. Blanks indicate that no measurements were possible, while colons indicate uncertain results.

We present this in a graphical form in Figure 11, together with the average count rates during orbital phase 0.04–0.09 ("post-eclipse flux"). The flux shows a clear modulation; moreover, the shape of the modulation suggest it has a ∼50 day period, indicative of a beat cycle phenomenon. As to the eclipse transition timings, there are instances of ingress and/or egress shifting earlier in phase over several weeks, with sudden jumps to a later phase, but it appears to have irregular variations as well.

We have then constructed two composite eclipse profiles. In one, we selected light curves for which we have been able to measure the ingress timings; we shift each curve to align the ingress before averaging the light curves. The other composite profile has the egress aligned. These are shown in Figure 12. These composite profile show sharp eclipse transitions, that ingress and egress times do not vary in concert, and that there may be two distinct emission regions.

The first point is obvious in the expanded views on the right half of Figure 12: the composite ingress is about 2.5 bins, or 5 s, while the composite egress is slightly longer (6–7 s). These numbers may be overestimates since our measurement errors can only blur the composite transitions. Although we cannot be sure that eclipse transitions are *always* sharp, it is clear that they often are. The sharpness also validates our measurement technique, and suggest that there is an intrinsic jitter in the accretion region location to cause the noisy appearance of Figure 11. The fact that the egress is gradual in the ingress-aligned composite profile (and vice-versa) shows that the two transitions do not move in step. Unless the accretion spot moves substantially within ∼ 700 s, this means that the eclipse width also varies. This interpretation is confirmed by Figure 13, in which we compare the average eclipse profiles of observations 1, 2, 13, and 14 (taken during days 0–5 and 50–55 of our campaign), against that of observations 3, 4, 5, 15, 16, 17 and 18 (days 8–16 and 58–66). The latter group has weaker out-of-eclipse emission (the part of the beat cycle during which the post-eclipse flux is steeply declining; see Figure 11), and hence it is difficult to measure the individual eclipses (note the blank and uncertain entries for these eclipses in Table 5). However, when combined, it becomes clear that there was an eclipse which was noticeably wider (∼750 s) than average. This can be explained if the location of the accretion region moves in latitude as well as in longitude (see §5.4). Finally, the egress-aligned composite (Figure 12) shows a slight rise, beginning about 0.01 cycle before the sharp egress, suggesting that a part of the X-ray emission region becomes visible about 120 s before the main emission region. However, this may well be due to a subset of the eclipses.

5. Discussion

5.1. Confirmation of the Eclipsing Nature of V1432 Aql

We have found that the X-ray eclipse is total, as observed with the imaging *BeppoSAX* MECS and *ASCA* GIS detectors. Therefore we have no doubt that this is not a dip due to accretion stream, but represents a true eclipse by the secondary, as Patterson et al. (1995) argued (see also Geckeler & Staubert 1999). This is contrary to the conclusion that Watson et al. (1995) reached, so it is important to examine where our disagreement originates.

Watson et al. (1995) have listed two reasons for believing that this was an accretion stream dip. One is that the optical eclipse light curve of V1432 Aql was unlike that of other eclipsing polars. We agree with this assessment, and interpret this simply as meaning V1432 Aql is unlike other polars, perhaps related to its asynchronous nature. The other reason is what they believed to be a residual flux from V1432 Aql during the eclipse, which was harder than the out-of-eclipse flux. Given that they based this on a non-imaging *Ginga* LAC observation pointed at NGC 6814 (see Figure 1), and given that our far more extensive X-ray data (both imaging and non-imaging) contradict this, we believe that the residual flux was in fact from NGC 6814 or yet another source in the LAC field of view. We believe that past non-imaging X-ray observations, particularly those which had NGC 6814 on-axis, are liable to be contaminated by this highly variable Seyfert galaxy, and cannot be re-interpreted as solely due to X-rays from V1432 Aql. At some epochs, as during the *ROSAT* All-Sky Survey (Figure 1), the AGN is brighter than the CV.

Our conviction is strengthened by the relative stability of the feature. A simple folding (Figure 10) results in a well-defined and sharp eclipse profile, with the only ill effect being the blurring of the transitions. This is consistent with an eclipse by the secondary of a small accretion region (or regions) moving about on the white dwarf surface; we do not believe that a stream dip in an asynchronous polar can be stable to this degree.

Given that the X-ray eclipse is by the secondary, we must also accept that the optical (Watson et al. 1995) and UV (Schmidt & Stockman 2001) eclipse is also by the secondary. This implies that the geometrical pattern of optical emission is unusual among polars, and that the UV continuum is not entirely due to the white dwarf photosphere, albeit with a superficial similarity. The accretion stream is a likely candidate for the additional source of optical and UV emission; this possibility should be investigated further using optical and/or UV data.

5.2. Inclination and the White Dwarf Mass

The eclipse width, customarily defined as time between mid-ingress and mid-egress, defines the relationship between the mass ratio q and the binary inclination i, if the eclipsed body is centered on the center of the white dwarf. Although this last assumption may be incorrect by up to the white dwarf radius for the X-ray emission region in V1432 Aql, an eclipse width of 695 s is indicative of $i \sim 75.7°$ for q=0.5 and $i \sim 77.7°$ for q=0.35 (Figure 14). In constructing this plot, we have used the Roche-lobe shape, as in Bailey (1979).

Further, we take the 85 s egress duration in the average *RXTE* profile (Figure 10) to be the result of the accretion region shifting on the white dwarf surface. This can be translated into a minimum size of the white dwarf, hence its maximum mass, using a white dwarf mass-radius relationship[3]. In the upper panel of Figure 14, we plot the full duration of the egress as a function of q, for two assumed values of mass of the secondary. In this and subsequent calculations, we have replaced the Roche lobe with a sphere that exactly reproduces the q–i relationship, given the 695 s eclipse duration, to speed up the calculation. The solid line is for the secondary mass $M_2 = 0.31\ M_\odot$, corresponding to a normal main sequence mass-radius relationship. For the maximum theoretical duration not to exceed the observed duration of 85 s, q must be less than 0.52, or the primary mass $M_1 < 0.59\ M_\odot$. For a 0.22 $M_\odot$ secondary (its radius R_2 of 1.2 × a main sequence star of the same mass), then the q limit shifts considerably, but the limit for M_1 remains about the same. Thus we conclude that the white dwarf in V1432 Aql is not particularly massive.

Although this conclusion is not warranted if the X-ray emission arises high above the white dwarf surface (thus allowing the location to move by much more than one white dwarf diameter), this is difficult to reconcile with the compact size of the X-ray emission region implied by the rapid eclipse transitions (Figure 12). The only way around this dilemma would be a vertically compact region high above the white dwarf surface (i.e., with little X-ray emission lower down); however, we consider this rather unlikely on theoretical grounds. If we take the combined durations of ingress and egress in the aligned profile (Figure 12) of 12 s to be the maximum contribution from the vertical extent of the emission region, and subtract it from 85 s, we still require a large, low-mass primary with an estimated upper limit of 0.67 $M_\odot$. This contradicts the estimate of 0.98 $M_\odot$ (90% confidence range of 0.78–1.19 $M_\odot$), based on the partial covering cold absorber fit to the the *RXTE* spectrum of V1432 Aql (Ramsay 2000), and implies the presence of hitherto unaccounted-for source(s) of systematic errors in either or both methods of X-ray based mass determination.

---

[3]We have used the convenient formula in Pringle & Webbink (1975). Use of alternative formulae, or the effects of different composition or core temperature, do not affect our conclusions significantly.

The wider eclipse sometimes seen can be most easily explained if the location of the observed X-ray emission shifted in latitude. This could be caused either by accretion switching from one pole to the other, or, if both poles are accreting all the time, by one pole going behind the white dwarf limb and the other coming into view. The required shift to widen the eclipse from 700 s to 750 s is of the order of 6000 km, comparable to the radius of the white dwarf (R_1). Such a large shift suggests that the dominant source of X-rays is associated with the magnetic pole on the upper hemisphere (when the eclipse width is ∼700 s) and with the lower pole when the width is wider (see §5.4 for further discussion). If this is true, then the above binary inclinations are somewhat (by a few 10th of a degree) underestimated.

5.3. Size of the Accretion Spot

How many accretion spots do we see? Whereas multiple spots cannot be ruled out, we do not have any clear instances of two sharp ingresses or two sharp egresses. That is, the X-rays observed near orbital phase 0.0 appear to be always dominated by a single spot. However, the eclipse experiment can only find an accretion spot on the hemisphere facing the secondary. We infer the presence of at least one more accretion spot from the fact that V1432 Aql does not have a faint phase in which hard X-rays are essentially undetected, as observed in several polars.

The ingress and egress durations in the aligned profiles (Figure 12) constrain the size of the dominant accretion spot facing the secondary. In the directions perpendicular to the secondary's edge at ingress and egress, the spot size is roughly 1100 km by 1600 km for a 0.62 $M_\odot$ primary and a 0.31 $M_\odot$ secondary (or 0.13 R_1 by 0.19 R_1); the numbers change to 1300 km by 1900 km (0.20 by 0.29) for a 0.87$M_\odot$ primary. This is much larger than found in normal, phase-locked polars. For example, in HU Aqr, Schwope et al. (2001) report an eclipse egress of only 1.3 s, corresponding to 450 km. In the only X-ray eclipsing IP, XY Ari, Hellier (1997) found an egress of 2 s.

The above values concur with the traditional picture that normal polars should have the smallest spots, since they accrete from a stream with a small cross-sectional area. It has previously been supposed that IP accretion areas will be much bigger, since the partial accretion disk might feed accretion over a much larger range of azimuth. However, the XY Ari value is much close to that for HU Aqr than that for V1432 Aql. This can be explained if the stream in polars punches into the magnetopshere and is stripped over a range of radii, while disk-fed accretion in IPs is from a smaller range of radii, compensating for any larger range of azimuth (Hellier 1999).

In V1432 Aql, both effects could be combining to produce the much larger accretion area. It is stream fed, leading to a range of stripping radii, but the accretion flow also has a large azimuthal extent (§5.5). The accretion may switch from pole to pole, and this non-stable nature could contribute to the disorganized state of the accretion, further increasing the accretion footprint. However, if this is the case, we might expect the larger spot size to lead to lower temperature of the soft component. In contrast, Friedrich et al. (1996) estimates a high temperature (kT=60±35 eV for the blackbody component in a bremsstrahlung plus blackbody fit) from the *ROSAT* PSPC spectrum of V1432 Aql, compared with a typical PSPC-measured temperature of ∼30 eV (Ramsay et al. 1994). Although these are not necessarily inconsistent (soft X-rays could originate in a small region within the larger envelop defined by the hard X-ray eclipse light curves), further studies are necessary to clarify the situation.

5.4. Movement of the Accretion Spot

The gradual shifting-forward of ingress/egress timings over ∼20 day period suggests that the accretion region is moving retrogradely in the co-rotating frame of the binary. Moreover, the fundamental period indeed appears to be ∼50 days. These are consistent with the asynchronous polar model of V1432 Aql, and are inconsistent with two of the three versions of the IP model of Mukai (1998). Although one version of the IP model is consistent with our data, the confirmation of the $\dot{P}$ of the 12,150 s period strongly favors the asynchronous polar model. The inferred synchronization timescale of $\sim$ 120 yrs is comparable to that for V1500 Cyg (Schmidt et al. 1995), while we naively expected a clear difference for V1432 Aql in which accretion and synchronization torques cooperates (unlike in other asynchronous Polars in which they compete; Mukai 1998). Clearly, we still have much to learn about the synchronization torques in asynchronous polars. Moreover, if all asynchronous polars are recent novae, such a rapid synchronization timescale would suggest a short ($\sim$ 2000 yrs) nova recurrence time for polars, which in turn leads to some difficulties (Warner 2002).

Given the high inclination of V1432 Aql, it is rather unlikely that a single accretion spot can remain in view throughout a spin cycle. For a rotational co-latitude of the spot β', this requires $i + \beta' < 90°$; since $i \gtrsim 75°$, it requires $\beta' \lesssim 15°$ (cf. the study of optical spin minima by Staubert et al. 2003). Any accretion spots having a β' greater than $\sim 15°$ must disappear behind the white dwarf limb; the relative lack of spin modulation in the hard X-rays (Figure 7) suggests that this is compensated for by the appearance of the other pole. A lack of hard X-ray spin modulation in V1432 Aql is not a total surprise, since there is a precedent in the flaring state of the well-known asynchronous polar, BY Cam (Ishida et al.

1991).

In Figure 15, we schematically plot the movement of these accretion spots as seen from Earth at mid-eclipse. In this plot, we assume two diametrically opposed spots, moving in longitude but staying constant in latitude. This is a simplification: while the magnetic poles are expected to move this way, the offset between the accretion spot and the magnetic pole changes as a function of the magnetic pole orientation (Mukai 1988; Geckeler & Staubert 1997). Because we cannot fully model this without more observational constraints, we will use this as a crude model. Furthermore, we assume that both spots accrete at all times, and we observe the region that is not hidden behind the white dwarf limb. In this schematic, the only asymmetry between the upper and lower poles is introduced by the viewing geometry (that is, $i \neq 90°$). For this plot, we use q=0.55, i=74.88°, and β'=45°.

Such a model makes a specific prediction for the X-ray eclipse timings. To facilitate a better comparison with this model, we have re-analyzed the *RXTE* eclipse timing by first combining light curves taken at similar beat phase. For this purpose, we use the beat period of 52 days appropriate for 1998, based on our ephemerides (1) and (2), and use HJD 2450940.99 as relative beat phase 0.0[4]. We then measured the ingress and egress phases in these 8 light curves, with higher signal-to-noise than in individual eclipses; we were able to measure all 8 X-ray ingresses and 7 of 8 egresses. These, and the resultant eclipse duration, are plotted as a function of this relative beat phase in Figure 16. Overplotted are the prediction of the model shown in Figure 15, for which beat phase 0.0 is defined as when the upper pole is most directly facing the secondary. We emphasize that this is not a fit; although the phasing works approximately correctly, this fortuitous agreement nevertheless appears to be imperfect. The choice of β' was adjusted by hand to reproduce the gross features of the data, but no formal fitting was performed. In particular, we note that this reproduces the fact that there is one jump to later phase in each timing, with a gradual shift forward for the rest of the cycle. For the ingress, this corresponds to the jump from the disappearance of the lower pole to the left and the appearance of the upper pole to the right. The change from upper pole to lower pole produces little shift, however, given this geometry, and vice versa for the egress timing. We believe this geometry provides a reasonable framework for more quantitative modeling of the X-ray eclipse timings in V1432 Aql.

When two spots are observed in turn during a beat cycle, a sudden changes in eclipse duration is predicted (Figure 16), although our particular model ovepredicts the amount. In comparison, the single spot model of Geckeler & Staubert (1997) predicts a gradual shift

[4]This is an arbitrary epoch for beat phase 0.0, chosen simply because it is the time of the first well-measured eclipse in our 1998 optical campaign, to be reported in a future paper.

with a total amplitude of $< 20°$. The shift required by the data is ∼6000 km (§5.2), or at least $\gtrsim 40°$ in latitude, depending on the primary mass. We therefore consider it rather secure that the eclipse timing data, which is sensitive to the projected displacement of the emitting region, requires the presence of two hard X-ray emitting spots. The spin modulation, on the other hand, is caused by the angular dependence of emission. Hard X-rays are probably emitted uniformly, whereas the optical emission is likely beamed. Our result, therefore, does not necessarily contradict that of Geckeler & Staubert (1997).

We have used an arbitrary epoch to define a relative beat phase for our data, which appears to be close (Figure 16) to the one shown in Figure 15. That is, at our relative beat phase 0.0, the upper pole points roughly towards the secondary. In contrast, Geckeler & Staubert (1997) have defined beat phase 0.0 as when the magnetic pole points most directly at the threading region. Using the epoch derived by Staubert et al. (2003) and our spin ephemeris (Eq. 2), our beat phase 0.0 appears to correspond to beat phase ∼0.2 in the system of Geckeler & Staubert (1997). This can be interpreted as reflecting the average position of threading region in V1432 Aql, which in many polars leads the secondary by a similar amount.

5.5. The Nature of the Orbital Modulation

There are two orbital dips in the *BeppoSAX* light curves of V1432 Aql, near orbital phase 0.2 and 0.65 (Figure 7). Although neither persists throughout the beat cycle, when they are present, their location appears roughly fixed in the orbital frame rather than in the spin frame. What are they, and what can they tell us about the accretion geometry of V1432 Aql?

First, we suspect these are the causes of the complex appearances of the power spectra, including the strong peak at about 4000 s, of the *ROSAT* data of V1432 Aql (Mukai 1998). The fact that these appear to be an orbital, rather than a spin, phenomenon is an additional evidence against the IP interpretation.

However, the phasing of these dips are reminiscent of that of dipping low-mass X-ray binaries (see, e.g., Smale et al. 1992). If this analogy is real, then V1432 Aql may have a ring of material circulating around the white dwarf, something akin to a partial accretion disk. In this picture, the accretion stream from the secondary hits the ring, creating the dip-causing structure at phase 0.65. The splashed material hits the ring again at phase 0.2, causing a secondary dip. Regardless of the validity of such a picture, it does appear necessary for an accretion stream to go around the white dwarf 80% of the way before being captured by the

magnetic field. Similar inference has also been made from optical emission line observations (Friedrich et al. 2000). We further speculate that such a ring might be responsible in part for the unusual optical eclipse light curves and of the optical eclipse timing variations. It appears that we have plenty to learn about the accretion processes in V1432 Aql and other asynchronous polars.

6. Conclusions

We draw the following conclusions from our study of V1432 Aql and NGC 6814 using our *RXTE* campaign as well as archival *ASCA* and *BeppoSAX* data:

(1) NGC 6814 is a variable source of 2–10 keV X-rays, occasionally reaching a few times 10^{-11} ergs s^{-2}cm^{-2} level. The levels seen during 1993–1994 with *ROSAT* and *ASCA* appear to be the faintest it was ever seen. Variability on the timescale of days and longer, and with amplitude of a factor of a few, is well-established.

(2) Non-imaging observations of NGC 6814 cannot therefore be reinterpreted as that of V1432 Aql. These data contain unknown mixtures of X-rays from both V1432 Aql and NGC 6814, and the latter can be brighter than the former.

(3) V1432 Aql is an eclipsing system beyond doubt, with an eclipse width of 695 s. Moreover, the X-ray source is small and moves around on the face of the white dwarf.

(4) The total range of movement suggests a low-mass white dwarf, less than 0.59 $M_\odot$, if the X-ray emission is on the surface, or 0.67 $M_\odot$ allowing for as much vertical extent as we think reasonable. These are lower than inferred from the modeling of its X-ray spectrum.

(5) When the individual ingress is aligned before stacking the light curves, it reveals a sharp ($\leq$ 5 s) ingress. Ditto for egress (6–7 s). This suggests an accretion region, with an area of less than 1% of the total surface area of the white dwarf, but larger than the spots in the IP, XY Ari, or in the polar, HU Aqr.

(6) The movement of the accretion spot is consistent with that expected for an asynchronous polar in which the spin period is slightly longer than the orbital period. We do not have a quantitative understanding, however, since there are currently too many free parameters.

(7) There are two orbital dips in addition to the eclipse in the *BeppoSAX* light curves of V1432 Aql, when folded on the orbital period. This suggests that some of the accreting matter travels most of the way around the white dwarf before being threaded by the primary's

magnetic field.

This research has made use of *BeppoSAX* and *ASCA* data obtained from the High Energy Astrophysics Science Archive Research Center (HEASARC), provided by NASA's Goddard Space Flight Center. We acknowledge the use of NASA's *SkyView* facility (http://skyview.gsfc.nasa.gov) located at NASA Goddard Space Flight Center in the production of Figure 1. We thank the *RXTE* operations team for their effort in scheduling these highly constrained observations, and the PCA team for their help in deciphering the collimator response. We also acknowledge the many observers of the Center for Backyard Astronomy network whose observations were essential in tracking the periods of V1432 Aql.

REFERENCES

Bailey, J. 1979, MNRAS, 187, 645

Boella, G., Butler, R.C., Perola, G.C., Piro, L., Scarsi, L. & Bleeker, J. 1997a, A&AS, 122, 299

Boella, G., Chiappetti, L. Conti, G., Cusumano, G., Del Sordo, S., La Rosa, G., Maccarone, M.C., Mineo, T., Molendi, S., Re, S., Sacco, B. & Tripiciano, M. 1997b, A&AS, 122, 327

Boller, T., Brandt, W.N. & Fink, H. 1996, A&A, 305, 53

Boller, Th, Brandt, W.N., Fabian, A.C. & Fink, H.H. 1997, MNRAS, 289, 393

Bradt, H.V., Rothschild, R.E. & Swank, J.H. 1993, A&AS, 97, 355

Cropper, M. 1990, Space Sci. Rev, 54, 195

Done, C. & Magdziarz, P. 1998, MNRAS, 298, 737

Doroshenko, V.T. 1988, Astrofizika, 28, 233

Elvis, M., Lockman, F.J. & Wilkes, B.J. 1989, AJ, 97, 777

Friedrich, S., Staubert, R., Lamer, G., König, M., Geckeler, R., Bässgen, M., Kollatschny, W., Östreicher, R., James, S.D. & Sood, R.K. 1996, A&A, 306, 860

Friedrich, S., Schwarz, R., Schwope, A., Staude, A., Geckeler, R. & Staubert, R. 2000, Abstracts of Contributed Talks and Posters presented at the Annual Scientific Meeting of the Astronomische Gesellschaft, Vol 17

Geckeler, R.D. & Staubert, R. 1997, A&A, 325, 1070

Geckeler, R.D. & Staubert, R. 1999, Abstracts of Contributed Talks and Posters presented at the Annual Scientific Meeting of the Astronomische Gesellschaft, Vol 15

Hellier, C. 1997, MNRAS, 291, 71

Hellier, C. 1999, in "Annapolis Workshop on Magnetic Cataclysmic Variables," eds. C. Hellier & K. Mukai (San Francisco: Astronomical Society of the Pacific), 1

Ishida, M., Silber, A., Bradt, H.V., Remillard, R.A., Makishima, K. & Ohashi, T. 1991, ApJ, 367, 270

Jahoda, K., Swank, J.H., Giles, A.B., Stark, M.J., Strohmayer, T., Zhang, W. & Morgan, E.H. 1996, in EUV, X-ray and Gamma-Ray Instrumentation for Astronomy VII, ed O.H. Siegmund (Bellingham, WA: SPIE), 59

King, A.R. & Williams, G.A. 1985, MNRAS, 238, 1029

König, M., Friedrich, S., Staubert, R. & Timmer, J. 1997, A&A, 322, 747

Madejski, G.M., Done, C., Turner, T.J., Mushotzky, R.F., Serlemitsos, P., Fiore, F., Sikora, M. & Begelman, M.C. 1993, Nature, 365, 626

Mittaz, J.P.D. & Branduardi-Raymont, G. 1989, MNRAS, 238, 1029

Mukai, K. 1988, MNRAS, 232, 175

Mukai, K. 1998, ApJ, 498, 394

Patterson, J 1994, PASP, 106, 209

Patterson, J., Skillman, D.R., Thorstensen, J. & Hellier, C. 1995, PASP, 107, 307

Peterson, B.M. et al. 2000, ApJ, 542, 161

Pringle, J.E. & Webbink, R.F. 1975, MNRAS, 172, 493

Ramsay, G. 2000, MNRAS, 314, 403

Ramsay, G., Mason, K.O., Cropper, M., Watson, M.G. & Clayton, K.l. 1994, MNRAS, 270, 692

Schmidt, G.D. & Stockman, H.S. 2001, ApJ, 548, 410

Schmidt, G.D., Liebert, J. & Stockman, H.S. 1995, ApJ, 441, 414

Schwope, A.D., Schwarz, R., Sirk, M. & Howell, S.B. 2001, A&A, 375, 419

Sekiguchi, K. & Menzies, J.W. 1990, MNRAS, 245, 66

Skillman, D.R. & Patterson, J. 1993, ApJ, 417, 298

Smale, A.P., Mukai, K., Williams, O.R., Jones, M.H. & Corbet, R.H.D. 1992, ApJ, 400, 330.

Staubert, R., König, M., Friedrich, S., Lamer, G., Sood, R.K., James, S.D. & Sharma, D.P. 1994, A&A, 288, 513

Staubert, R., Friedrich, S., Pottschmidt, K., Benlloch, S.,Schuh, S.L., Kroll, P., Splittgerber, E. & Rothschild, R. 2003, A&A, in press (astro-ph/0306072)

Tanaka, Y., Inoue, H. & Holt, S.S. 1994, PASP, 46. L37

Tananbaum, H. 1980, in "X-ray astronomy; Proceedings of the Advanced Study Institute, Erice, Italy, July 1-14, 1979," eds. R. Giacconi & G. Setti (Dordrecht: D. Reidel Publishing Co.), 291

Turner, T.J., Romano, P., George, I.M., Edelson, R., Collier, S.J., Mathur, S. & Peterson, B.M. 2001, ApJ, 561, 131

Verbunt, F., Bunk, W.H., Ritter, H. & Pfeffermann, E. 1997, A&A, 327, 602

Warner, B. in "Classical Nova Explosions," eds. M. Hernanz & J. José (Mellville: American Institute of Physics), 3

Watson, M.G., Rosen, S.R., O'Donoghue, D., Buckley, D., Warner, B., Hellier, C., Ramseyer, T., Done, C. & Madejski, G. 1995, MNRAS, 273, 681

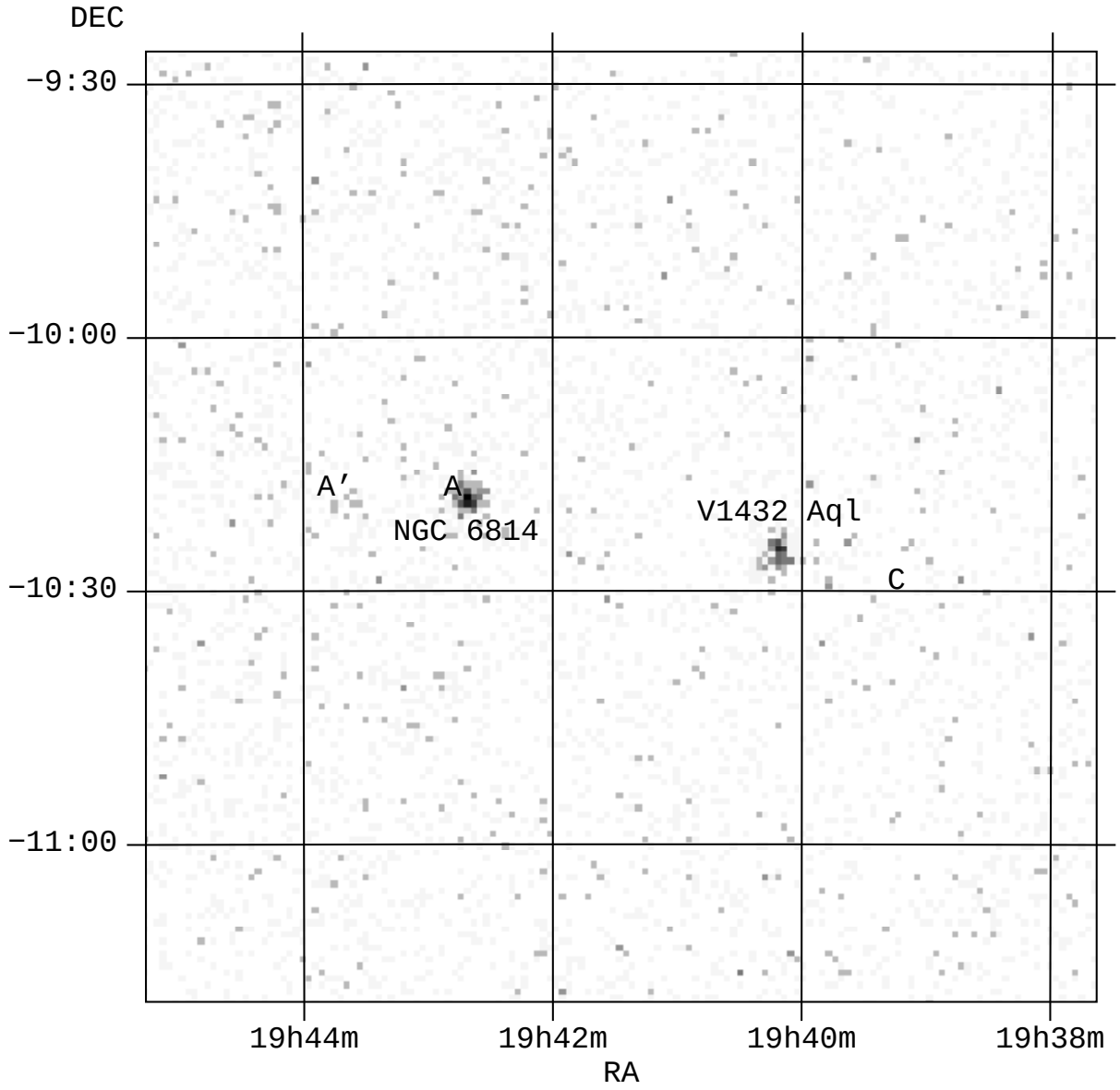

Fig. 1.— The *ROSAT* All-Sky Survey image of the region containing NGC 6814 (detected at 0.36 cts s^{-1}) and V1432 Aql (0.32 cts s^{-1}), marked with the pointing positions (A and C) used in our *RXTE* observing campaign. Also marked (A') is the intended pointing position (see text).

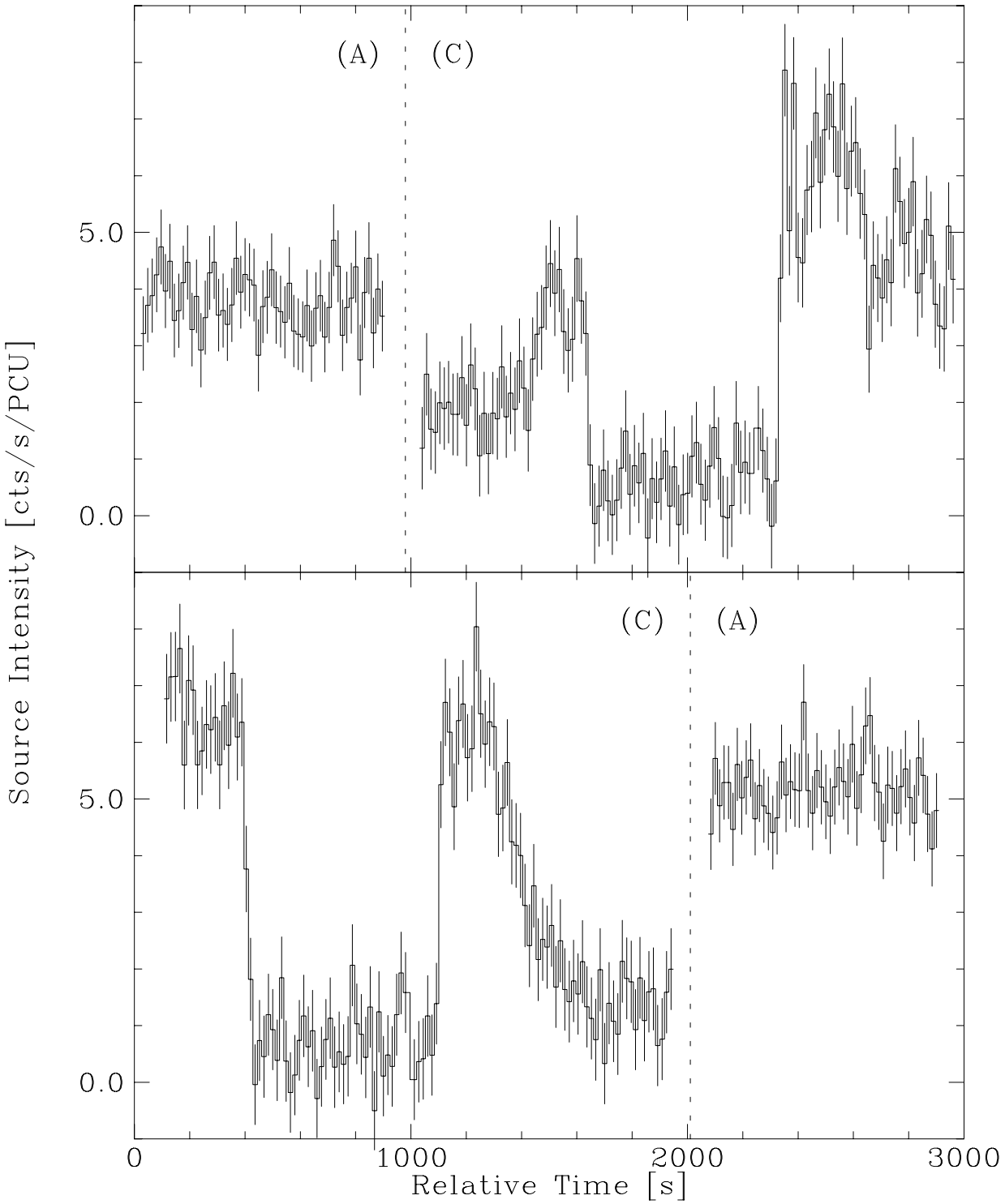

Fig. 2.— Light curves obtained at pointing positions A and C during the 1st and the 9th *RXTE* PCA observations, likely dominated by the NGC 6814 and V1432 Aql, respectively. The bin size is 16 s, and time 0 corresponds to 1998 May 18 at 12:58:00 UT (top) and 1998 June 19 at 19:21:40 UT (bottom), respectively.

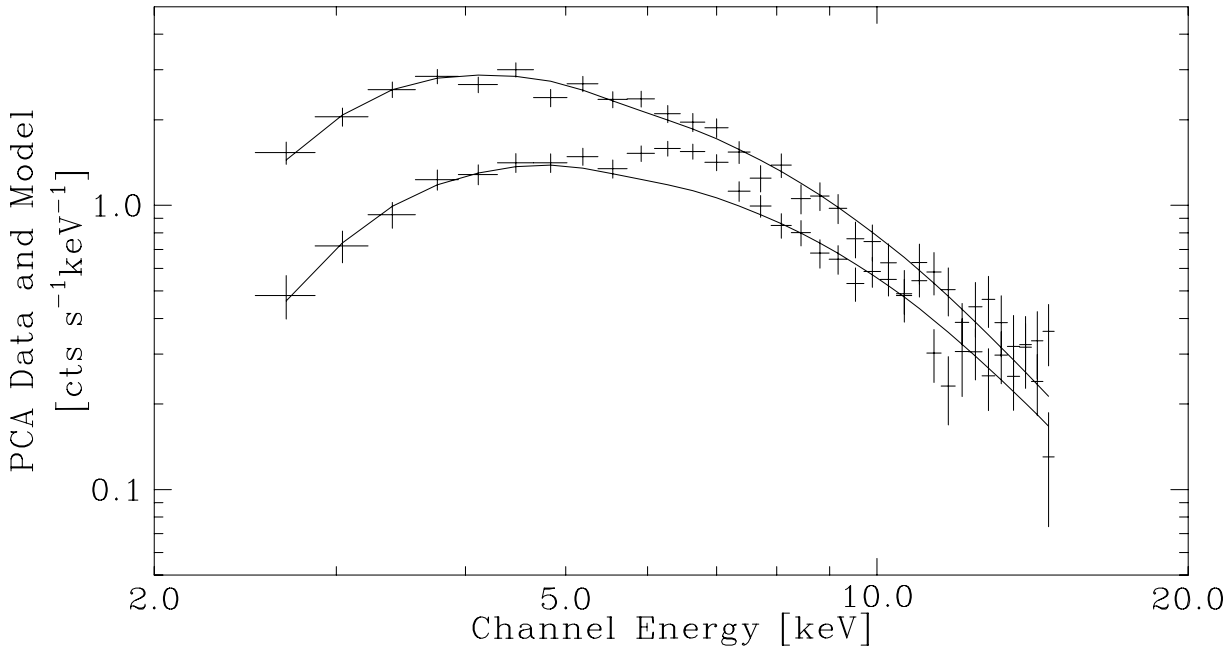

Fig. 3.— The spectra of NGC 6814 (brighter) and V1432 Aql (fainter) from the 1st *RXTE* PCA observation. Best-fit continuum models are also plotted, even though an Fe Kα is clearly required for the latter.

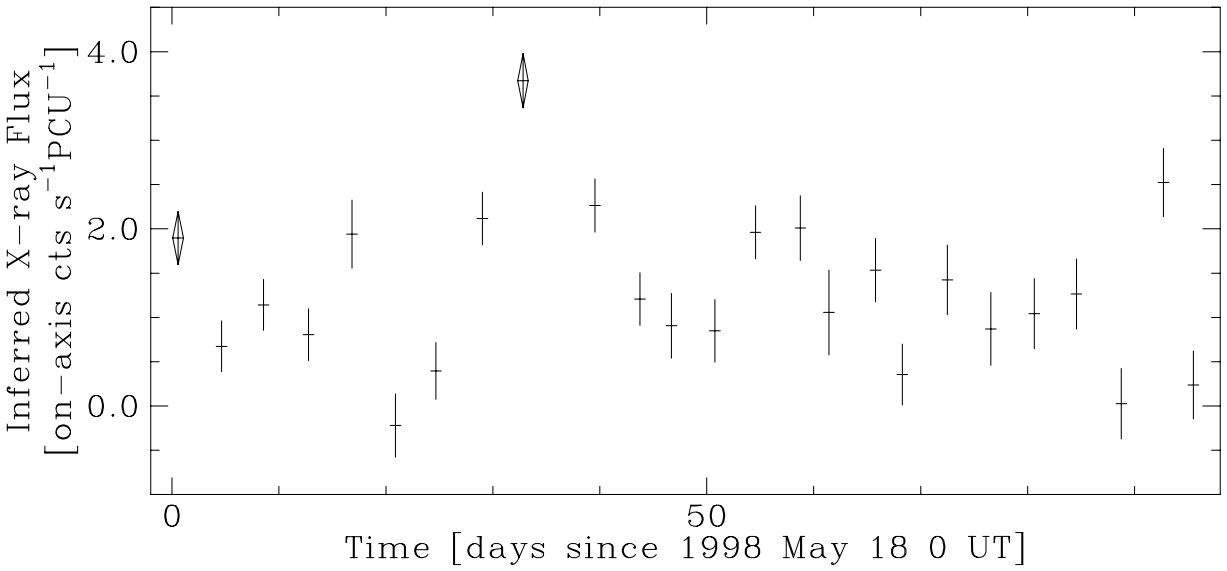

Fig. 4.— Inferred X-ray brightness of NGC 6814 (appropriate for on-axis *RXTE* observations), inferred from the average PCA count rate at mid-eclipse of V1432 Aql. Except for the two secure detections from "A" pointings (shown using combination diamond/plus symbols), these should be considered upper limits.

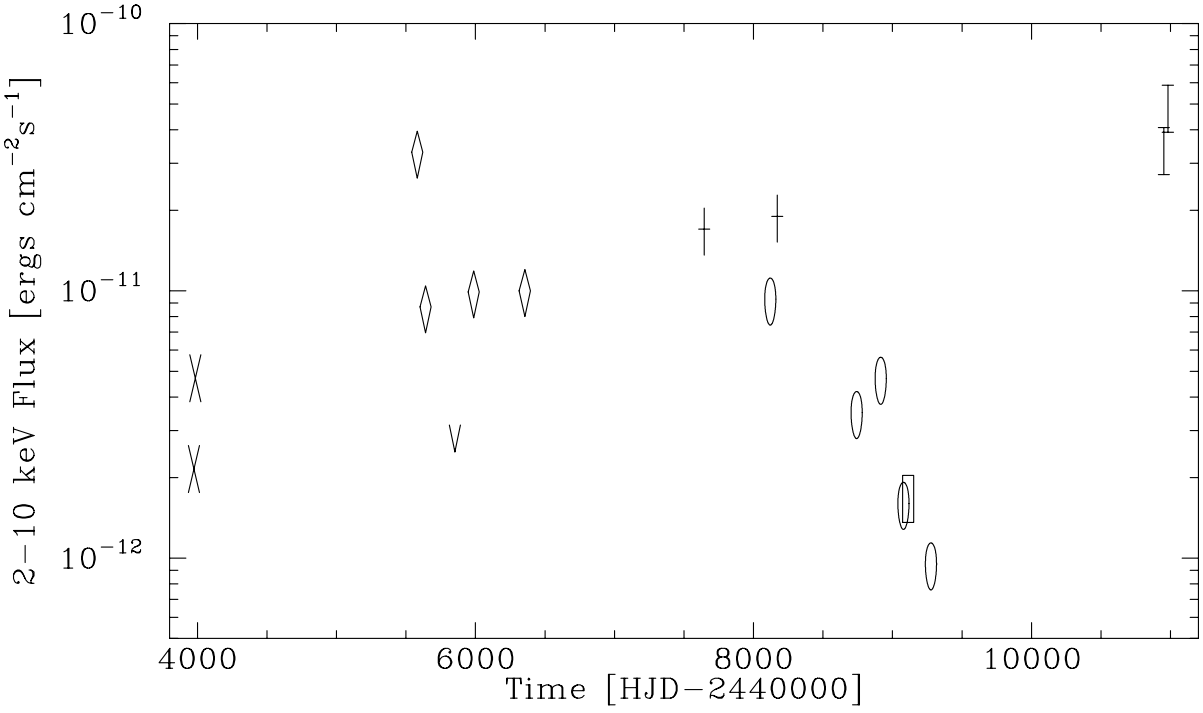

Fig. 5.— The long-term 2–10 keV flux history of NGC 6814 reconstructed from archival X-ray observations. Symbols are: Xes for *Einstein*, diamonds for *EXOSAT* detections and v for an *EXOSAT* upper limit, crosses for *Ginga*, ellipses for *ROSAT*, square for *ASCA*, and error bars for *RXTE* observations. See text for details including caveats on the reliability of various points.

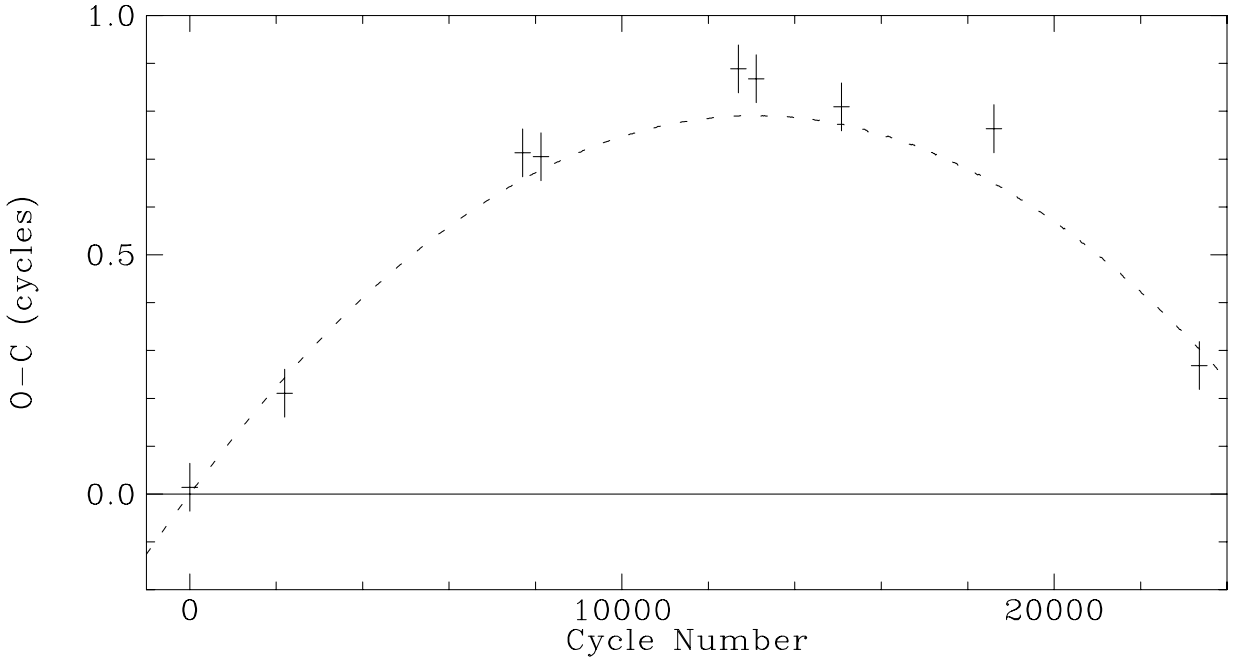

Fig. 6.— The O−C diagram of the times of spin minima, measured from CBA photometry (data given in Table 4), plotted as a function of cycle number relative to a test linear ephemeris, $HJD2449197.741 + 0.140613E$. Each point is the measured times averaged over a beat cycle. The dashed line is our best-fit quadratic ephemeris, which corresponds to a synchronization timescale of ∼120 years.

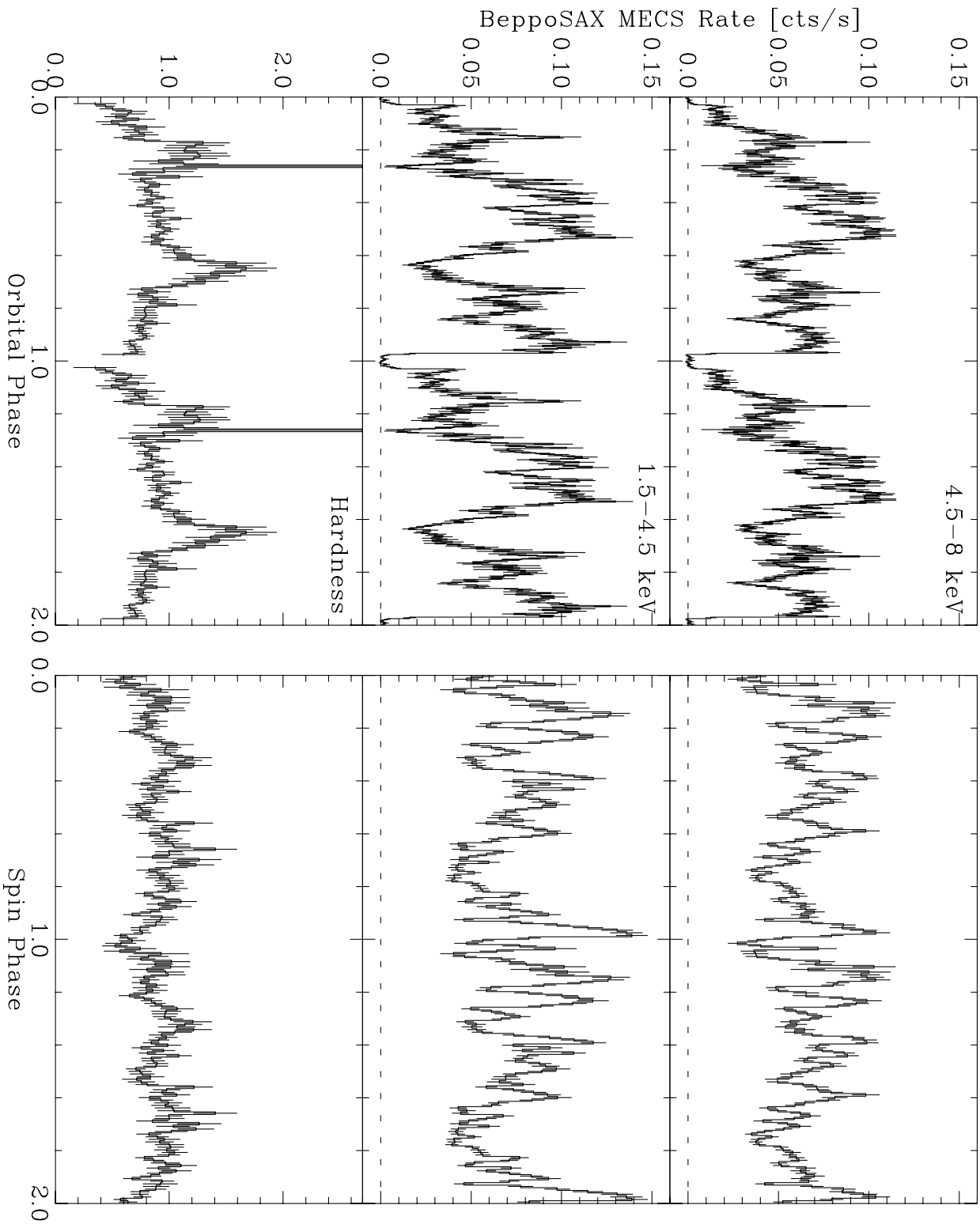

Fig. 7.— (Left) *BeppoSAX* light curves of V1432 Aql in two energy bands folded on the orbital period using ephemeris (1) (202 bins per cycle, or ∼60 s per bin), and the hardness ratio ([4.5–8 keV]/[1.5–4.5 keV], 101 bins per cycle, but undefined during eclipse), plotted twice for clarity. (Right) The same light curves, excluding orbital phase 0.95–1.10, folded on the spin period using ephemeris (2) (101 bins per cycle).

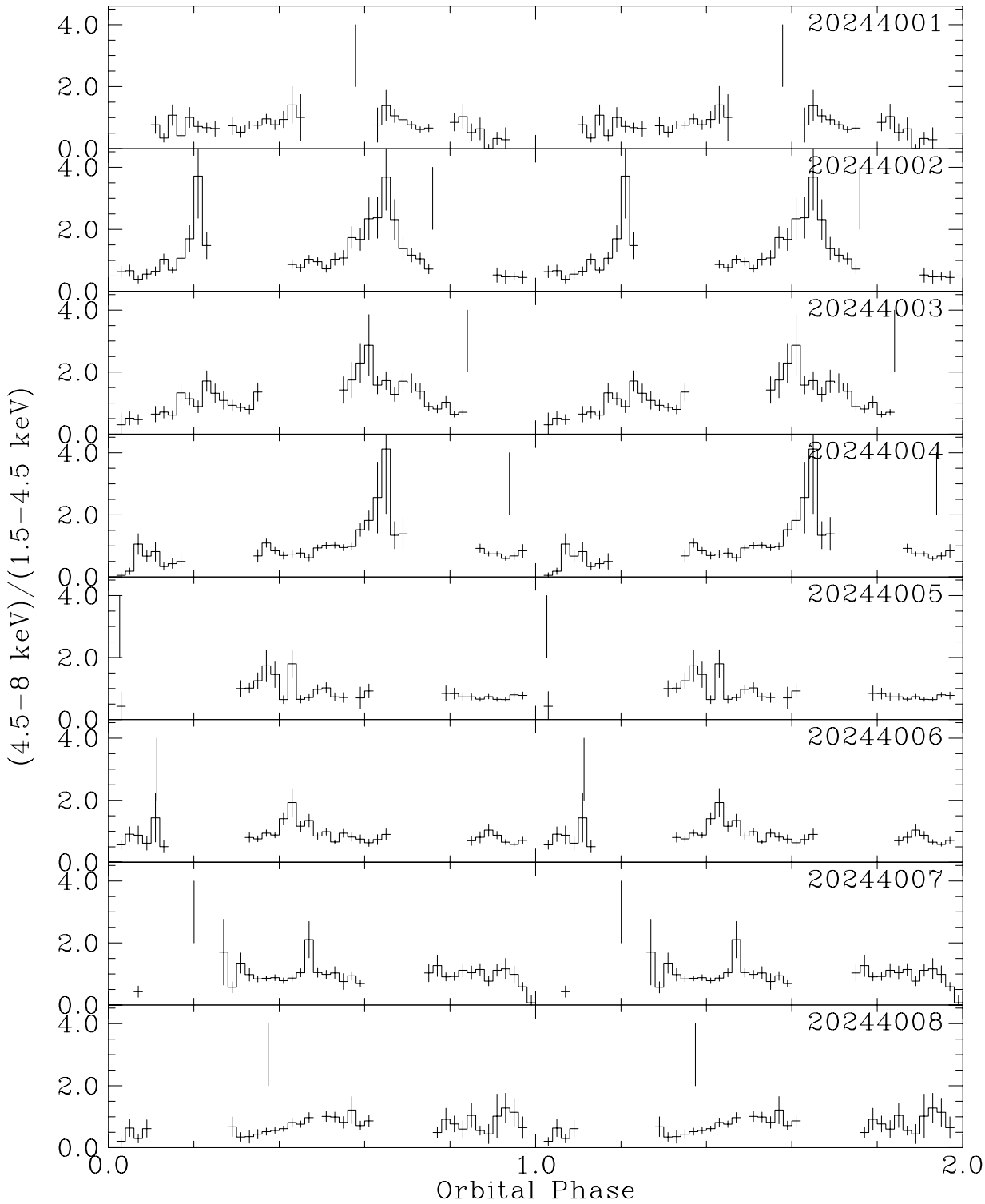

Fig. 8.— Hardness ratios for each of the 8 *BeppoSAX* observations folded on the orbital period (ephemeris (1); 50 bins per cycles, two cycles). Vertical bars indicate spin phase 0.0 using ephemeris (2). Although the data gaps complicate the comparisons, it can be seen that spectral hardening at phases 0.2 and 0.65 is variable (see text).

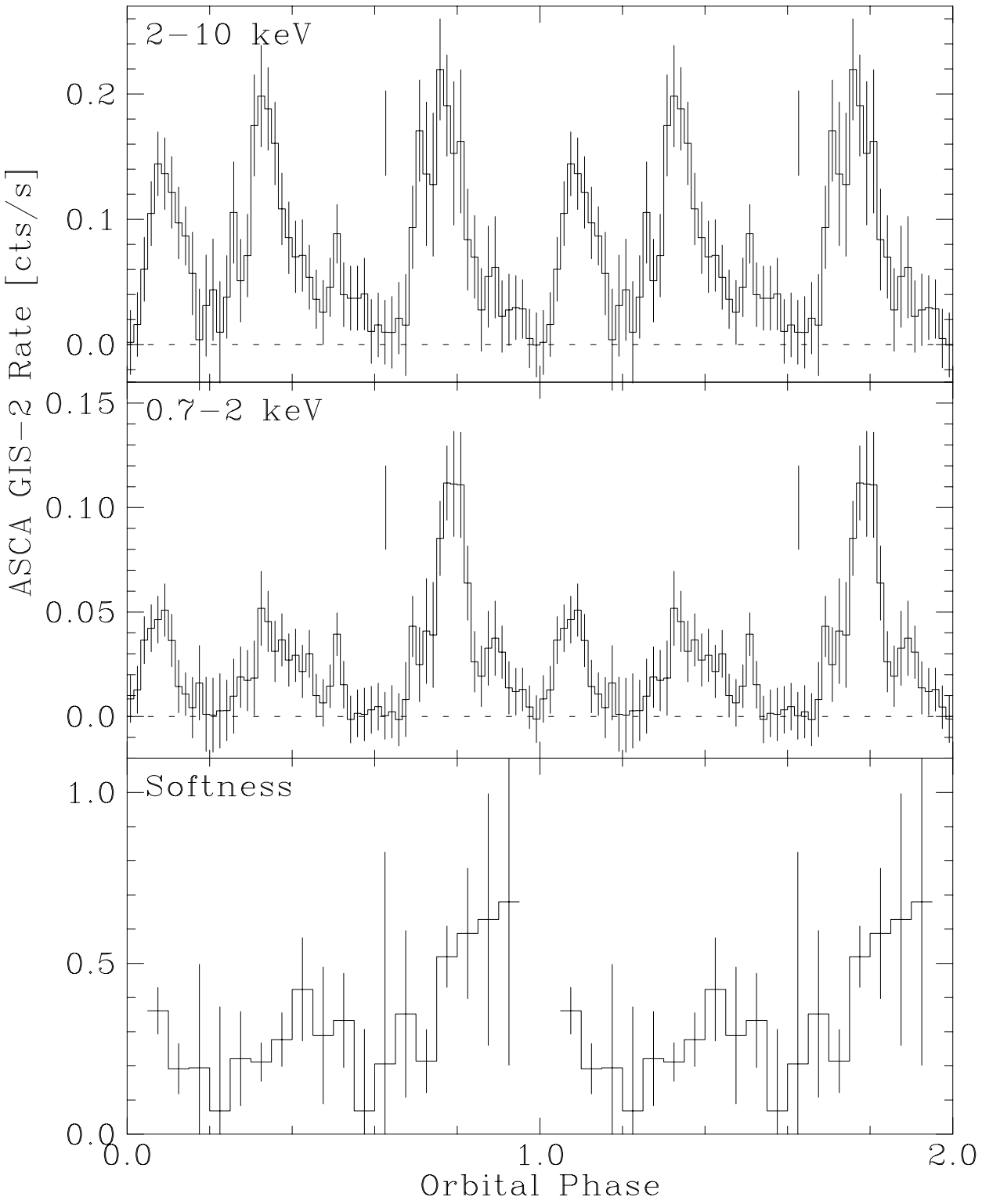

Fig. 9.— *ASCA* GIS-2 light curves in two energy bands folded on the orbital period using ephemeris (1) (120 bins per cycle, or ∼100 s per bin) and the softness ratio ([0.7–2 keV count rate]/[2-10 keV count rate], 20 bins per cycle), plotted twice. The vertical lines in the upper two panels indicate the expected orbital phase of the optical spin minimum during this observation, according to ephemeris (2).

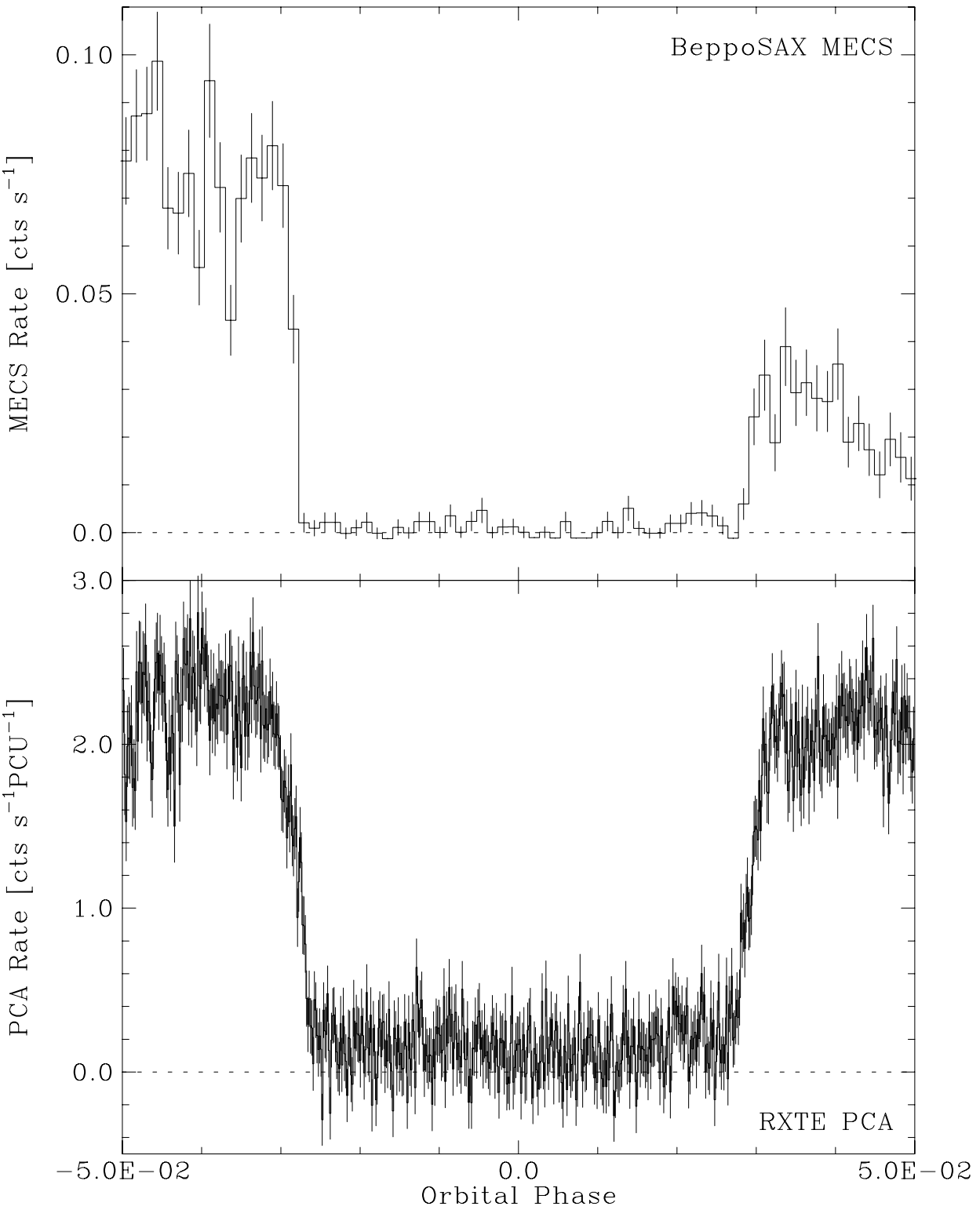

Fig. 10.— Folded *BeppoSAX* and *RXTE* light curves around phase 0.0 according to ephemeris (1), in 757 bins per orbital cycle (∼16 s per bin) for the *BeppoSAX* data, and 6058 bins per orbital cycle (∼2 s per bin) for the *RXTE* data. Dashed lines are drawn for a net count rate of 0.0.

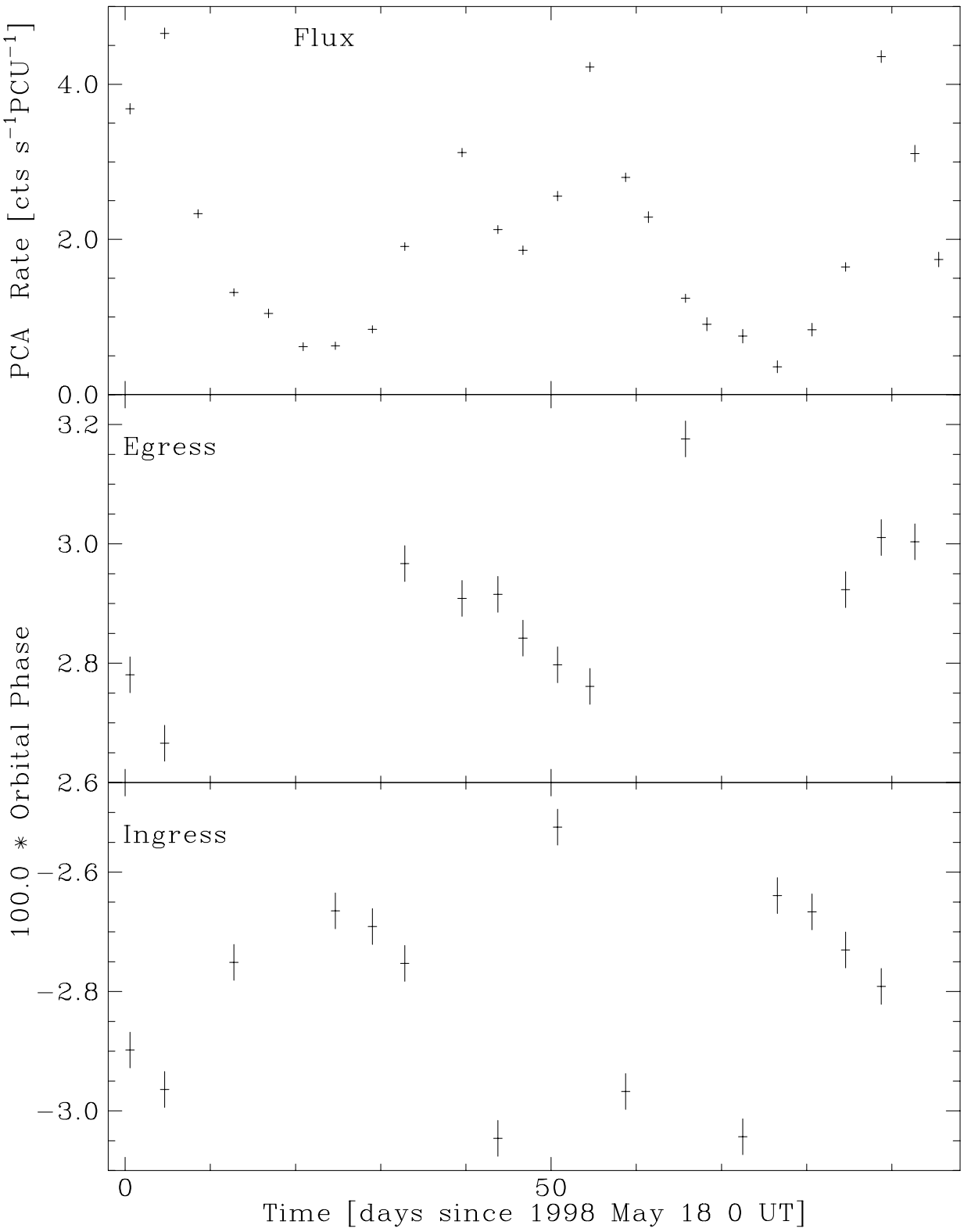

Fig. 11.— The out-of-eclipse flux (average count rate during orbital phase 0.04–0.09), and the ingress and egress timings (in units of 0.01 of an orbital cycle) are plotted against time through our *RXTE* observging campaign.

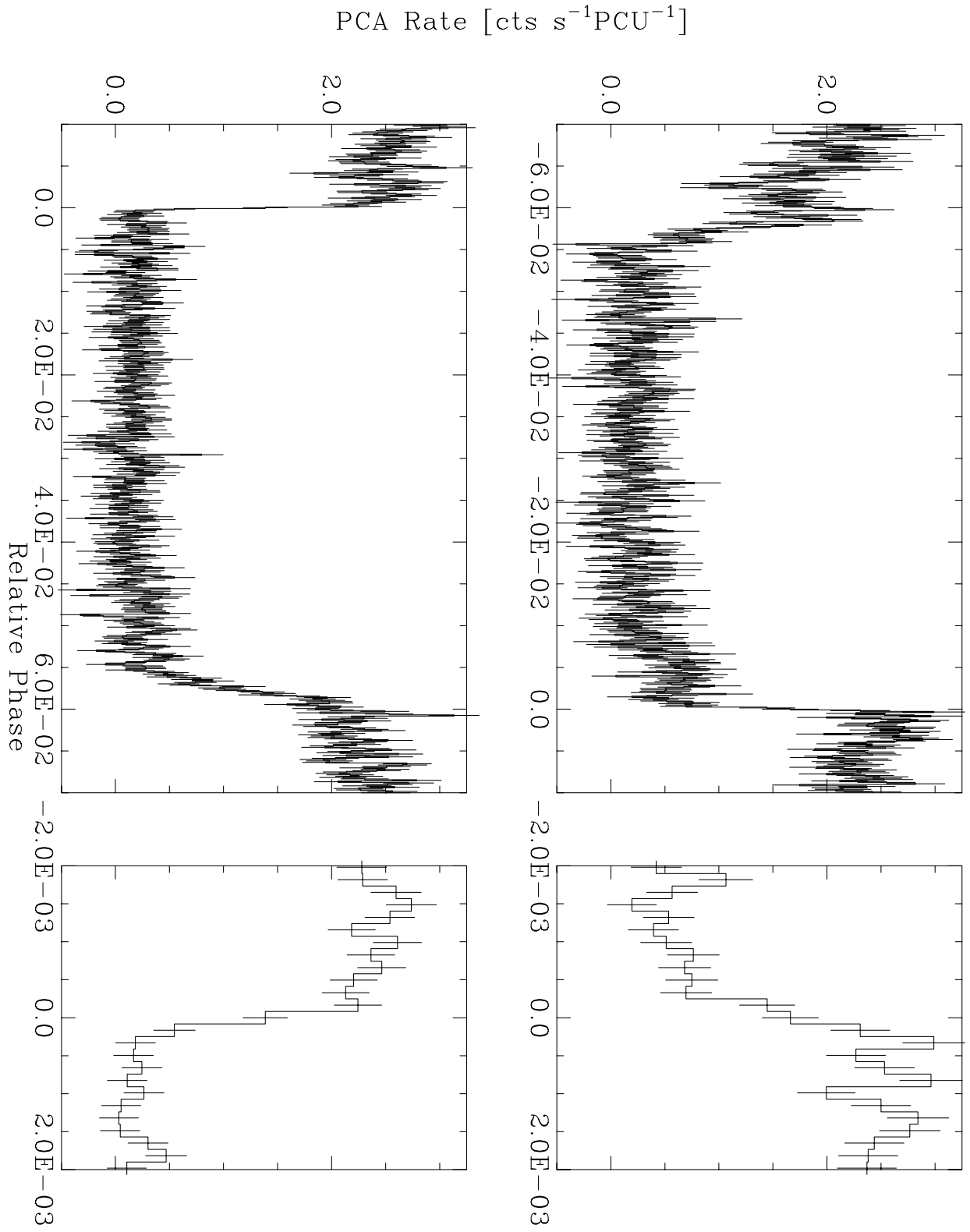

Fig. 12.— Folded light curves in ∼2 s bins, after manually aligning the ingress (lower panels) and egress (upper panels). For this figure only, we plot phase relative to the ingress (lower panels) or the egress (upper panels). The left side of the figure shows the overall eclipse shape, while detailed of the aligned feature is shown on the right.

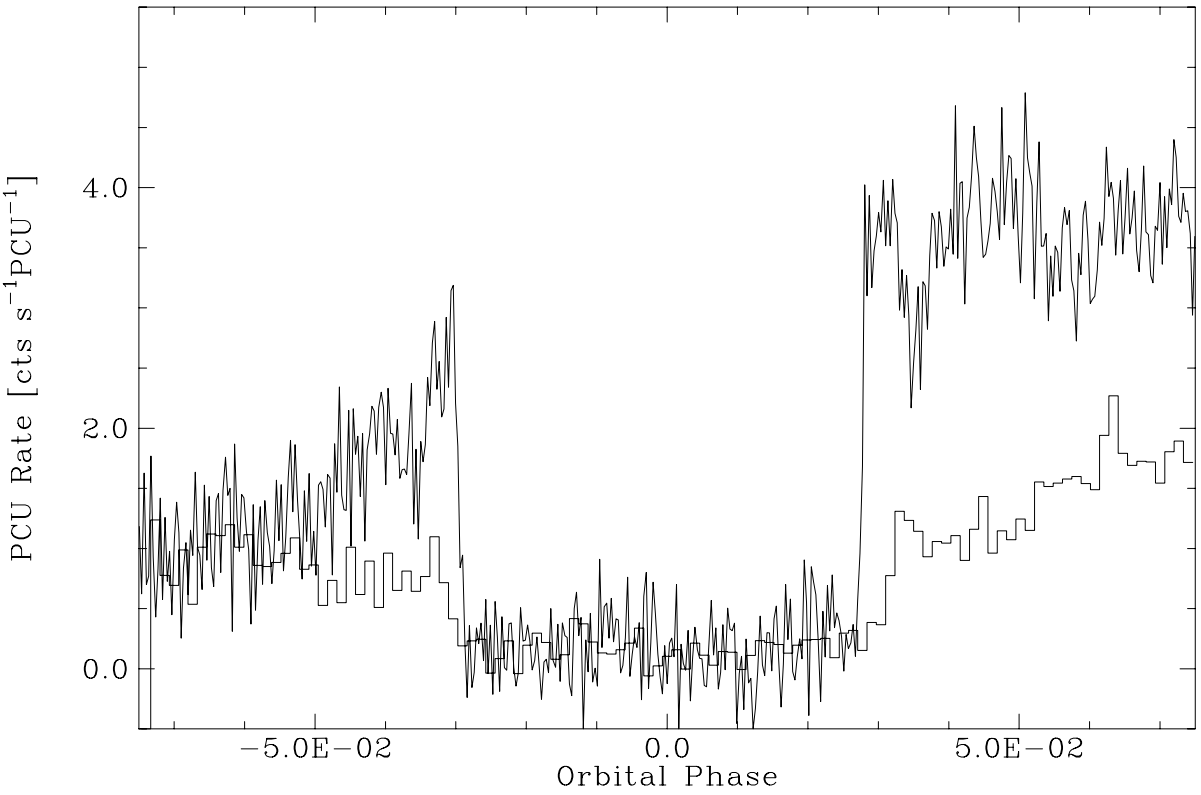

Fig. 13.— The average eclipse profile from observations 1, 2, 13, and 14 (line plot, in 4 s per bin), overplotted with the average eclipse profile from observations 3, 4, 5, 15, 16, 17, and 18 (histogram, in 16 s per bin). The latter are clearly wider than the former.

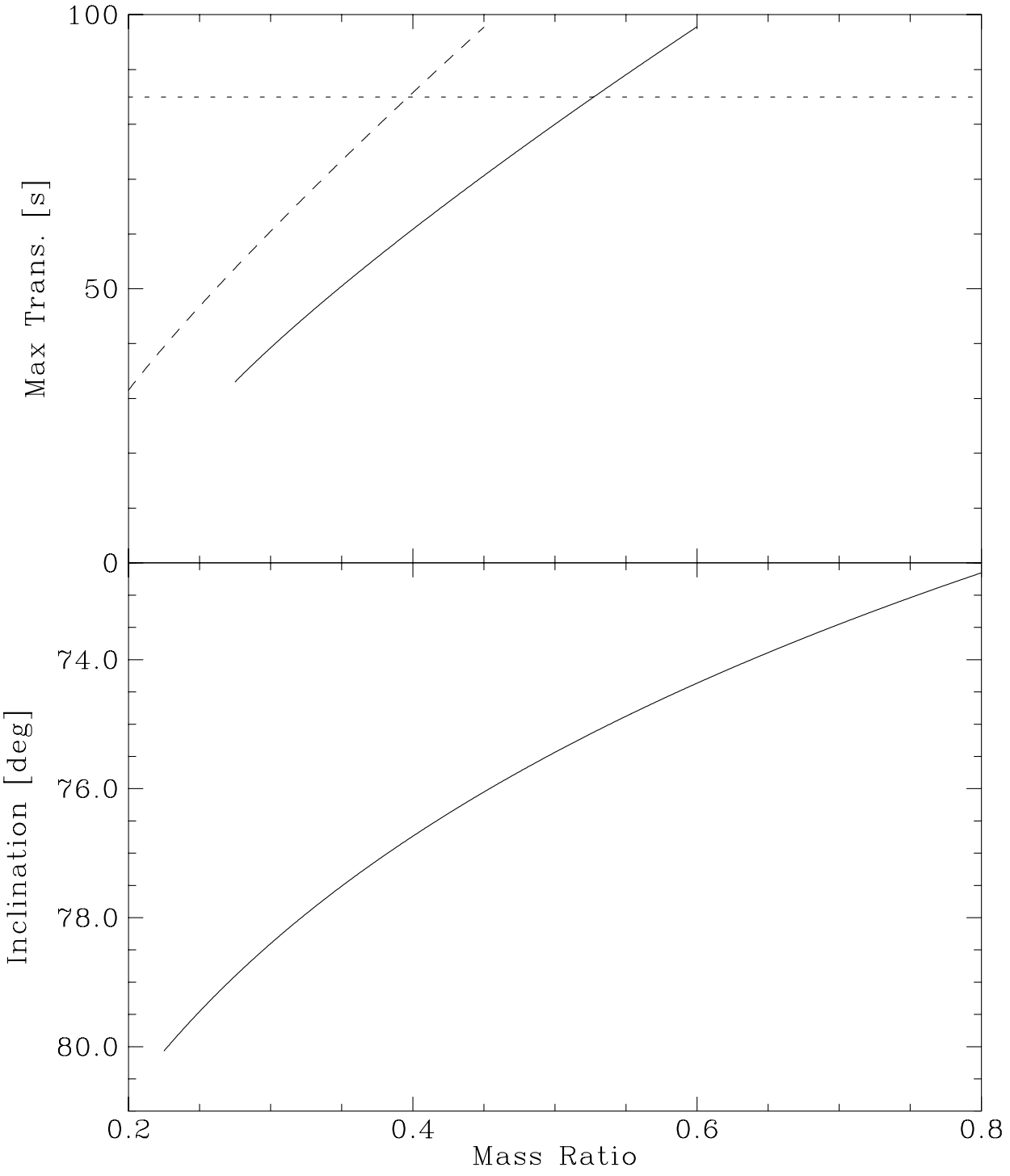

Fig. 14.— The inclination (i) mass-ratio (q) relationship for an eclipse width of 695 s is plotted in the lower panel. In the upper panel, maximum duration of eclipse transition is plotted as a function of q for two assumed secondary masses (solid line: 0.31 $M_\odot$; dashed line: 0.22 $M_\odot$). The dotted line is the observed egress duration in the average *RXTE* data, in which the transitions are smeared due to spot movement.

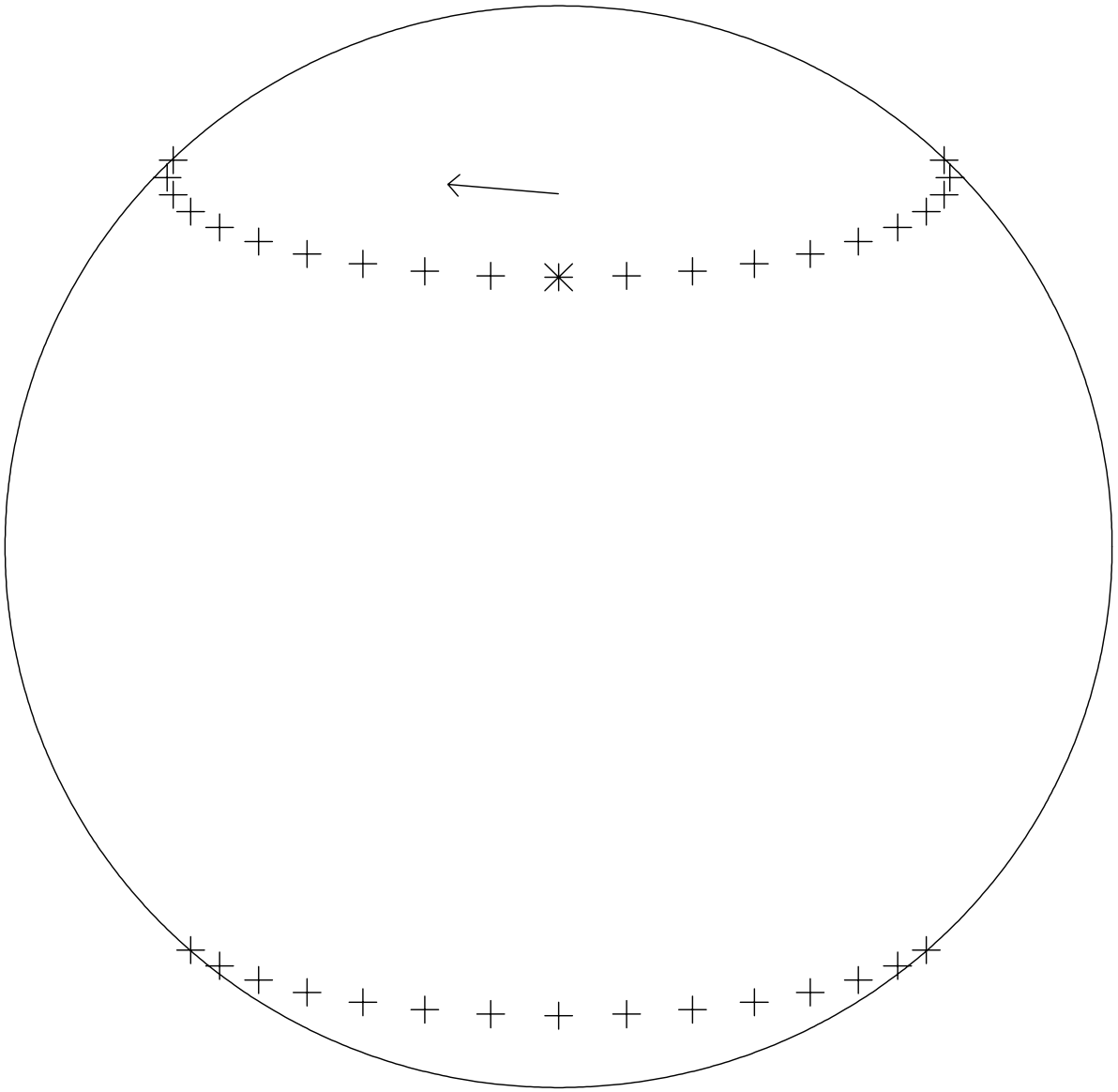

Fig. 15.— A schematic diagram of the accretion spot movement over a beat phase, as seen from Earth at orbital phase 0.0. The star is the position at an arbitrary beat phase 0.0. The spot moves left until it disappears and the lower pole appears to the bottom right. It moves left until it disappears and the upper pole reappears at top right. The limb of the secondary would be a line from upper left to lower right at ingress, moving right; and a right-moving line from upper right to lower left at egress.

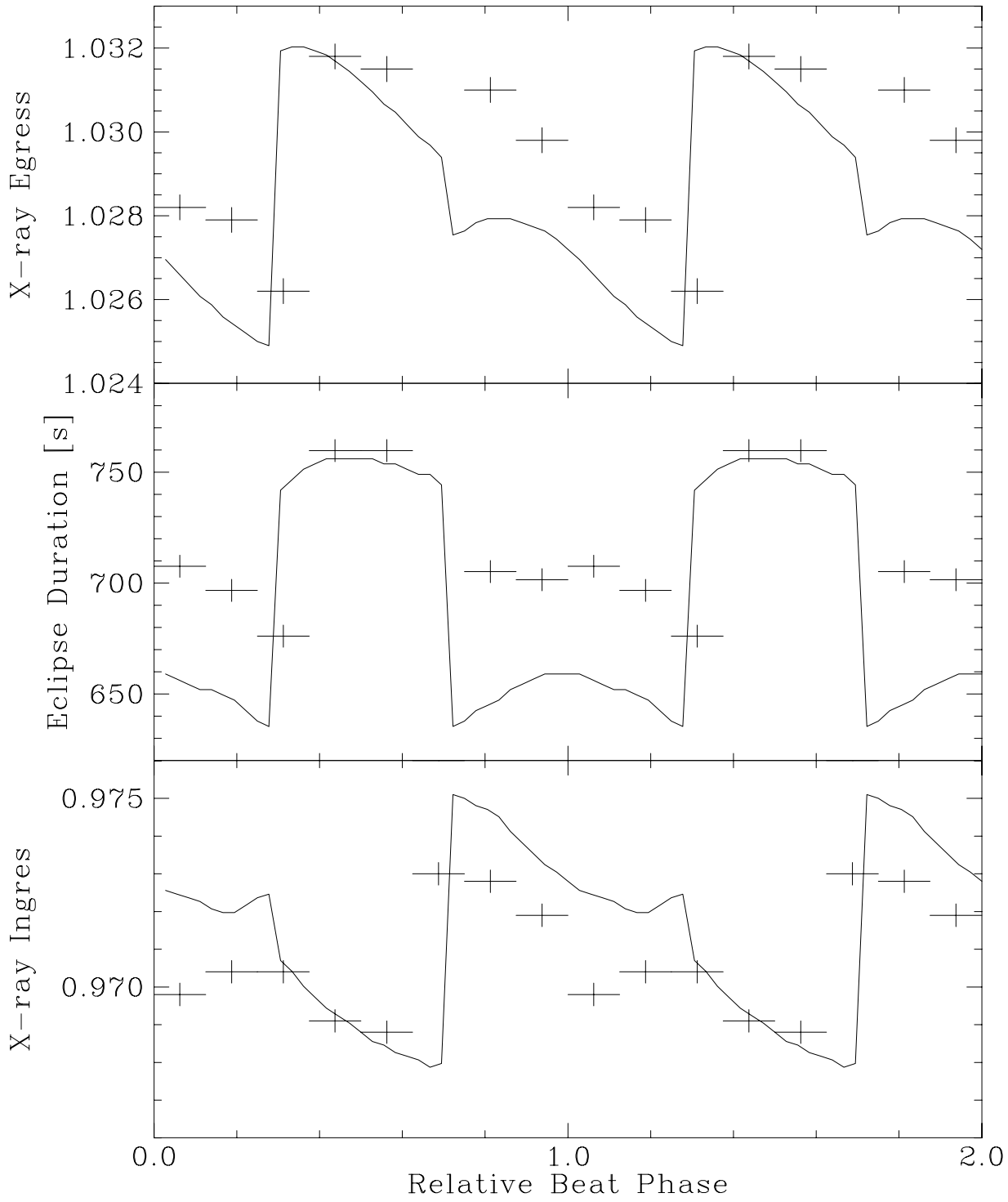

Fig. 16.— Ingress (bottom) and egress (top) timings (expressed in orbital phase) measured from average X-ray eclipse profiles in each of 8 beat-phase bins, and plotted twice for clarity. The middle panel shows the X-ray eclipse duration in seconds. For these points, we use a relative beat phase defined by a period of 52 days and a phase 0.0 at HJD 2450940.99. The lines in all three panels show the predictions of the schematic model (see text for details).

Table 1. Log of Imaging Observations

Satellite	Sequence no	Start Date & Time (UT)	End Date & Time	Exposure (ksec)
BeppoSAX	20244001	1997 Apr 02 06:50	Apr 02 11:50	9.1
	20244002	1997 Apr 11 16:36	Apr 11 22:35	12.2
	20244003	1997 Apr 15 21:42	Apr 16 02:37	10.0
	20244004	1997 Apr 20 20:02	Apr 21 01:40	12.3
	20244005	1997 Apr 25 11:10	Apr 25 16:19	8.4
	20244006	1997 Apr 29 19:51	Apr 30 03:00	12.9
	20244007	1997 May 04 10:02	May 04 15:21	10.8
	20244008	1997 May 13 05:44	May 13 11:05	9.5
ASCA	75009000	1997 Oct 27 20:25	Oct 29 00:11	39.6

Table 2. Target and Pointing Directions of the *RXTE* Campaign

	R.A. (2000)	Dec	Distance to V1432 Aql	Distance to NGC 6814
C	19 39 11.9	−10 27 49.0	14.84′	52.00′
V1432 Aql	19 40 11.47	−10 25 25.1		37.16′
NGC 6814	19 42 40.6	−10 19 24.6	37.16′	
A	19 42 46.2	−10 17 00.2	38.97′	2.77′

Table 3. The *RXTE* Campaign

ObsID[a]	Time[b] (Days)	Obs. Start[c] (UT)	End	Active PCUs	Pointings	Collimator Eff. for CV	Collimator Eff. for AGN
30015-01-01-00	0.6	May 18 13:13	14:00	01234	A–C	0.8036	0.1133
30015-01-02-00	4.6	May 22 14:50	15:27	01234	A–C	0.8039	0.1133
30015-01-03-00	8.6	May 26 13:08	14:08	01234	A–C	0.8036	0.1132
30015-01-04-00	12.8	May 30 18:04	19:14	01234	A–C	0.8036	0.1131
30015-01-05-00	16.8	Jun 03 19:43	20:41	0123	A–C	0.7811	0.1024
30015-01-06-00	20.9	Jun 07 21:18	22:10	0123	A–C	0.7806	0.1022
30015-01-07-00	24.7	Jun 11 16:13	16:43	01234	C–A	0.8018	0.1125
30015-01-08-00	29.0	Jun 16 00:31	01:37	01234	A–C	0.8013	0.1126
30015-01-09-00	32.8	Jun 19 19:23	19:54	01234	C–A	0.8008	0.1125
30015-01-10-00	39.5	Jun 26 12:59	13:33	01234	C–A	0.7982	0.1123
30015-01-11-00	43.8	Jun 30 17:48	18:26	01234	C–A	0.7966	0.1123
30015-01-12-00	46.7	Jul 03 16:31	17:06	0123	A–C	0.7718	0.1010
30015-01-13-00	50.8	Jul 07 18:12	18:42	0123	A–C–A	0.7675	0.1027
30015-01-14-00	54.6	Jul 11 13:05	13:39	01234	C–A	0.7837	0.1155
30015-01-15-00	58.8	Jul 15 18:05	18:32	01234	C–A	0.7786	0.1011
30015-01-16-00	61.4	Jul 18 09:55	10:29	012	C–A	0.7485	0.0865
30015-01-17-00	65.8	Jul 22 18:19	19:24	01234	A–C	0.7560	0.0981
30015-01-18-00	68.3	Jul 25 06:49	07:16	01234	C–A	0.7520	0.0939
30015-01-19-00	72.5	Jul 29 11:43	12:14	01234	A–C–A	0.7509	0.0870
30015-01-20-00	76.6	Aug 02 13:24	13:51	01234	C–A	0.7514	0.0853
30015-01-21-00	80.6	Aug 06 15:01	15:27	01234	C–A	0.7454	0.0839
30015-01-22-00	84.6	Aug 10 13:11	13:47	01234	C–A	0.7429	0.0844
30015-01-23-00	88.8	Aug 14 18:10	18:45	0123[d]	A–C	0.7468	0.0918
30015-01-24-00	92.7	Aug 18 16:22	16:54	01234	C–A	0.7396	0.0880
30015-01-25-00	95.5	Aug 21 11:33	12:13	01234	C–A	0.7405	0.0883

[a]Observation ID number assigned by the *RXTE* project for the "C" pointings.

[b]Time Since 1998 May 18 0 UT

[c]All observations listed were carried out in 1998.

[d]All 5 PCUs were operational during a part of this observation.

Table 4. Timings of Optical Spin Minima

Observing Season	Spin Minima (HJD)
1993	2449197.743
1994	2449506.838
1996	2450280.702
1996	2450340.602
1998	2450982.948
1998	2451040.737
1999	2451317.877
2000	2451813.672
2002	2452481.936

Table 5. The *RXTE* Campaign Results

ObsID	Cycle No[a]	$HJD_{mid-ecl}$ (predicted)	Ingress (cycle)	Egress (cycle)	Duration (s)	Post-ecl. Flux[b] (ct/s/PCU)
30015-01-01-00	12496	2450952.0664	−0.0290	+0.0278	688	3.68
30015-01-02-00	12525	2450956.1332	−0.0296	+0.0271	687	4.66
30015-01-03-00	12553	2450960.0598				2.33
30015-01-04-00	12583	2450964.2669	−0.0275:	+0.0288:	682:	1.32
30015-01-05-00	12612	2450968.3337		+0.0317:		1.05
30015-01-06-00	12641	2450972.4005				0.62
30015-01-07-00	12668	2450976.1868	−0.0269			0.63
30015-01-08-00	12699	2450980.5341	−0.0269	+0.0285:	671:	0.84
30015-01-09-00	12726	2450984.3204	−0.0275	+0.0297	693	1.91
30015-01-10-00	12774	2450991.0517	−0.0304:	+0.0291	721:	3.12
30015-01-11-00	12804	2450995.2587	−0.0305	+0.0291	722	2.13
30015-01-12-00	12825	2450998.2037	−0.0304:	+0.0284	713:	1.86
30015-01-13-00	12854	2451002.2705	−0.0297	+0.0280	699	2.56
30015-01-14-00	12881	2451006.0568	−0.0282:	+0.0276	676:	4.22
30015-01-15-00	12911	2451010.2639	−0.0297			2.80
30015-01-16-00	12930	2451012.9283	−0.0305:	+0.0329:	768:	2.29
30015-01-17-00	12961	2451017.2756	−0.0265:	+0.0318	706:	1.24
30015-01-18-00	12979	2451019.7998	−0.0314:	+0.0330:	780:	0.91
30015-01-19-00	13009	2451024.0069	−0.0304	+0.0295:	726:	0.75
30015-01-20-00	13038	2451028.0737	−0.0264			0.36
30015-01-21-00	13067	2451032.1405	−0.0267	+0.0319:	710:	0.84
30015-01-22-00	13095	2451036.0671	−0.0273	+0.0292	685	1.65
30015-01-23-00	13125	2451040.2741	−0.0279	+0.0301	703	4.36
30015-01-24-00	13153	2451044.2007	−0.0295:	+0.0300:	721:	3.11
30015-01-25-00	13173	2451047.0054				1.74

[a]Cycle number of the eclipse observed, as defined by our ephemeris (1).

[b]Average count rate during orbital phase 0.04–0.09.